國 立 交 通 大 學
材 料 科 學 與 工 程 學 系
博 士 論 文

離子氮化及氣體氮化對鐵鋁錳碳合金顯微結構、機械性質及抗腐蝕性質影響之研究

Microstructures, Mechanical Properties and Corrosion Behaviors of the Plasma-Nitrided and Gas-Nitrided Fe-Al-Mn-C Alloys

研 究 生：陳柏至
指導教授：劉 增 豐 博士
朝 春 光 博士

中 華 民 國 一 百 零 二 月 九 月

Microstructures, Mechanical Properties and Corrosion Behaviors of the Plasma-Nitrided and Gas-Nitrided Fe-Al-Mn-C Alloys

研 究 生：陳柏至　　Student: Po-Chih Chen

指導教授：劉增豐 博士　　Advisor: Dr. Tzeng-Feng Liu

朝春光 博士　　Dr. Chuen-Guang Chao

國 立 交 通 大 學

材 料 科 學 與 工 程 學 系

博 士 論 文

A Dissertation

Submitted to Department of Materials Science and Engineering

College of Engineering

National Chiao Tung University

in Partial Fulfillment of the Requirements

for the Degree of

Doctor of Philosophy

in

Materials Science and Engineering

Sep 2013

Hsinchu, Taiwan, Republic of China

中 華 民 國 一 百 零 二 年 九 月

誌　謝

由衷感謝的指導教授劉增豐博士與朝春光教授數年來悉心指導，使學生能夠順利完成此論文。兩位老師不僅只於學術上的指導，在行為處事上的教導，也使學生獲益匪淺，銘記在心。口試時承蒙莊振益教授、吳忠春博士、薄慧雲副所長等口試委員悉心指正，更令學生由衷感謝。

感謝我的父母與家人在這段時間對我的支持與鼓勵，雖然最疼愛我的母親無法親眼看到我完成學業的這一刻，但我相信她一定已經知道了這個消息而且會非常欣慰。

感謝實驗室眾多曾經一起共事過的夥伴們給我的幫助，尤其是楊小姐、志龍學長、凱明學長、世陽學長、浩仰、晟毅、育誠及明翰還有其他眾多曾經在鐵鋁錳實驗室的同學及在交大認識的朋友，在這裡一併致上最深的感謝。

最後，僅將論文獻給我最愛的父母親、家人，感謝他們多年來的辛勞、支持與鼓勵，使我能無後顧之憂地完成學業。

2013/9 於交大

離子氮化及氣體氮化對鐵鋁錳碳合金顯微結構、機械性質及抗腐蝕性質影響之研究

研究生：陳柏至　　指導教授：劉增豐 博士

朝春光 博士

國立交通大學材料科學與工程研究所

中文摘要

本論文主要分別研究離子氮化及氣體氮化對 Fe-8.68wt.%Al-30.5wt.%Mn-1.85wt.%C 和 Fe-9wt.%Al-28wt.%Mn-1.8wt.%C 合金之顯微結構、機械性質與抗腐蝕性質影響。依據實驗的結果，本論文所得到的具體研究結果如下:

（一）Fe-8.68wt.%Al-30.5wt.%Mn-1.85wt.%C 的淬火結構為沃斯田鐵相(austenite, γ)，且在γ基地內有十分緻密奈米級(nano-sized)的$(Fe,Mn)_3AlC$ 碳化物(κ'-碳化物)。緻密奈米級的κ'-碳化物是合金在固溶化淬火過程中藉由史賓諾多分解(spinodal decomposition)相變化在γ基地內形成。將在淬火狀態下的 Fe-8.68wt.%Al-30.5wt.%Mn-1.85wt.%C 合金，經 500℃、8 小時離子氮化處理後，在γ基地內的κ'-碳化物會成長且量變多，而使氮化後合金能具有優異的強度和延性組合，且在合金表面可得到 40 μm

厚的氮化層，此氮化層結構由 X 光繞射可知，主要組成為具有面心立方(Face-Centered Cubic, F.C.C)之 AlN 及少量的 FCC Fe_4N；藉由離子氮化處理後的 Fe-8.68wt.%Al-30.5wt.%Mn-1.85wt.%C 合金表面氮濃度高達 20wt.%(48 at.%)。所以表面硬度可高達 1860 Hv，基材硬度為 550 Hv，延伸率為 33.6%，且在 3.5%鹽水中具有極佳抗腐蝕性質，這些特性都遠優於一般經最佳氮化處理後的高強度合金鋼，工具鋼，麻田散鐵不銹鋼及析出硬化型不銹鋼。

（二）Fe-9wt.%Al-28wt.%Mn-1.8wt.%C 的淬火結構為沃斯田鐵相(austenite, γ)，且在γ基地內有十分緻密奈米級(nano-sized)的$(Fe,Mn)_3AlC$ 碳化物(κ'-碳化物)。緻密奈米級的κ'-碳化物是合金在固溶化淬火過程中藉由史賓諾多分解(spinodal decomposition)相變化在γ基地內形成。在淬火狀態下，Fe-9wt.%Al-28wt.%Mn-1.8wt.%C 合金經 500℃、8 小時和 50%NH_3+50% H_2 氣氛氣體氮化處理後，表面可得到約 31 μm 厚的氮化層，此氮化層結構由 X 光繞射可知，主要組成為 AlN 及少量的 Fe_4N；氣體氮化後表面氮濃度高達 17 wt.% (~41 at.%)；藉由氣體氮化處理的 Fe-9wt.%Al-28wt.%Mn-1.8wt.%C 合金，表面硬度可高達 1700 Hv，基材硬度 550 Hv，延伸率為 33.2%，且在 3.5%鹽水中具有極佳抗腐蝕性質，這些特性都遠優於一般經最佳離子氮化及氣體

氮化處理後的高強度合金鋼，工具鋼，麻田散鐵不銹鋼及析出硬化型不銹鋼。經由研究發現，氣體氮化試片經拉伸測試後，表面氮化層與基材間仍有極佳的附著性，不易脫落。此外，藉由氣體氮化後試片角落無明顯的電弧效應現象產生，而此現象在一般離子氮化處理過程中始終是難以避免的。

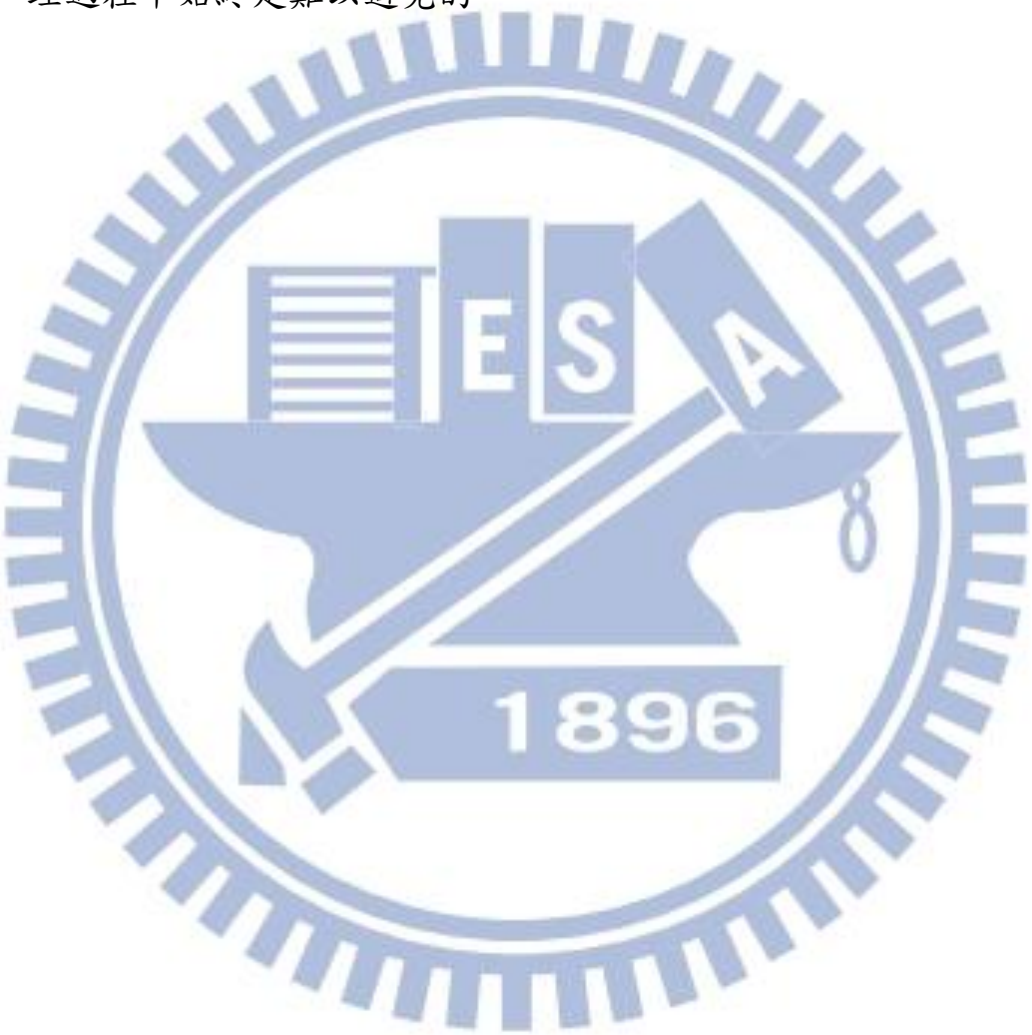

Microstructures, Mechanical Properties and Corrosion Resistance of Plasma-Nitrided and Gas-Nitrided Fe-Al-Mn-C Alloys

Student: Po-Chih Chen **Advisor: Dr.Tzeng-Feng Liu**

Dr. Chuen-Guang Chao

Department of Materials Science and Engineering

National Chao Tung University

Abstract

The as-quenched Fe-8.68wt.%Al-30.5wt.%Mn-1.85wt.%C alloy was plasma-nitrided at 500°C for 8h with 50% N_2 and 50% H_2 atmosphere under a pressure of 130Pa, and the as-quenched Fe-9wt.%Al-28wt.%Mn-1.8wt.%C alloy was gas-nitrided at 500°C for 8h using an atmosphere of 50% NH_3 and 50% H_2, respectively. Microstructures, mechanical properties and corrosion behaviors of the plasma-nitrided Fe-8.68wt.%Al-30.5wt.%Mn-1.85wt.%C and gas-nitrided Fe-9wt.%Al-28wt.%Mn-1.8wt.%C alloys have been investigated. On the basis of the experimental examinations, some results can be summarized as follows:

[1]. The as-quenched microstructre of the Fe-8.68wt.%Al-30.5wt.%Mn-1.85 wt.%C alloy was austenite (γ) phase containing an extremely high density of nano-sized $(Fe,Mn)_3AlC$ carbides (κ'-carbide). These κ'-carbides were formed within austenite matrix by spinodal decomposition during quenching. The size and the amount of the κ'-carbides increased dramatically when the as-quenched Fe-8.68wt.% Al-30.5wt.% Mn-1.85 wt.% C alloy was plasma-nitrided at 500°C for 8h. Consequently, the nitrided alloy could obtain an excellent combination of strength and ductility after being plasma-nitrided. The nitrided layer obtained is 40 μm-thick and composed predominantly of F.C.C AlN with a small amount of Fe_4N. Due to the surface nitrogen concentration reached up to 20wt.% (48at.%), the surface hardness (1860 Hv), substrate hardness (550 Hv), ductility (33.6%), and corrosion resistance in 3.5% NaCl solution in the plasma-nitrided Fe-8.68wt.% Al-30.5wt.% Mn-1.85 wt.% C alloy are far superior to those obtained previously in optimally nitrided high-strength alloy steels, as well as martensitic and precipitation-hardening stainless steels.

[2]. The as-quenched microstructre of the Fe-9wt.%Al-28wt.%Mn-1.8wt.%C alloy was austenite (γ) phase containing an extremely high density of

nano-sized $(Fe,Mn)_3AlC$ carbides (κ'-carbide). These κ' carbides were formed within austenite matrix by spinodal decomposition during quenching. The as-quenched Fe-9wt.%Al-28wt.%Mn-1.8wt.% C alloy was directly gas-nitrided at 500°C for 8h with 50%NH_3+50% H_2 atmosphere, resulting in a ~30 μm-thick nitrided layer. The nitrided layer consists predominantly of nano-crystalline AlN with a small amount of Fe_4N. The nitrogen concentration at surface was extremely high up to ~17 wt.% (~41 at.%) . Consequently, the surface microhardness (1700Hv), substrate hardness (550Hv), ductility (33.2%) and corrosion resistance in 3.5% NaCl solution of the present gas-nitrided Fe-9wt.%Al-28wt.%Mn-1.8wt.% C alloy are far superior to those obtained previously for the optimally gas-nitrided or plasma-nitrided high-strength alloy steels, as well as martensitic and precipitation-hardening stainless steels. Moreover, it is very novel that the nitrided layer almost remained coherent and adhered well with the matrix after tensile test. Additionally, the present gas nitriding appeared to overcome the edge effects commonly encountered in plasma nitriding treatments for metals.

Contents

List of Tables

List of Figures

Chapter 1.

General Introduction

General introduction

Phase transformations, mechanical properties and corrosion resistance in fully austenitic Fe-(4.9~11)Al-(28~35)Mn-(0.5~1.3)C alloys have been extensively studied by many workers [1-40]. In the Fe-Al-Mn-C alloy systems, manganese and carbon can enhance the stability of the austenitic structure which has a better workability and ductility. Aluminum is a ferrite stabilizer and plays an important role on the formation of $(Fe,Mn)_3AlC$ carbides (κ′-carbides). An increase in the aluminum content will be beneficial to the mechanical strength of the alloys. In general, the F.C.C. structure can be stabilized by increasing the contents of the manganese and carbon, or decreasing the content of the aluminum. It is well-known that through a proper combination of aluminum, manganese and carbon, an alloy with a fully austenitic structure can be achieved.

In previous works, it is clearly demonstrated that the as-quenched microstructure of the FeAlMnC alloys with a chemical composition in the range of Fe-(6-11)wt.%Al-(26-34)wt.%Mn-(0.54-1.3)wt.%C was single-phase austenite (γ). When the as-quenched alloys were aged at 500~750℃ for moderate times, fine and coarse $(Fe,Mn)_3AlC$ carbides having an $L'1_2$-type structure could be observed to precipitate coherently within the γ matrix and heterogeneously on the γ/γ grain boundaries, respectively. For convenience, the κ′ carbide and κ carbide were used to represent the $(Fe,Mn)_3AlC$ carbide formed

coherently within the γ matrix and heterogeneously on the γ/γ grain boundaries [8]. In the previous studies, it was seen that the κ carbide has an $L1_2$-type structure [37-40]. However, Sarreal and Koach suggested that the κ-carbide has an $L1_2$ or $L'1_2$ structure [37]. The only difference between the $L1_2$ and $L'1_2$ structure is the degree of order of the carbon atom arrangement. The carbon atoms are randomly situated on octahedral site for the $L1_2$ structure, while they are all located in the body-centered, octahedral site for the $L'1_2$ structure, as shown in Figure 1.1. Based on these previous studies, it can be generally concluded that due to the formation of the fine k′ carbides within the γ matrix and absence of precipitates on the grain boundaries, the alloys could possess an optimal combination of strength and ductility when the as-quenched alloys were aged at 550℃ for about 16 h [8-10, 14]. With an elongation better than about 30%, the values of UTS and YS could be attained to be 1130-1250 MPa, 1080-1120 MPa and 33-31%, respectively [8-10, 14-15].

Recently, in order to further improve the strength, small amounts of V, Nb, Mo and W were added to the austenitic FeAlMnC (C ≦ 1.3 wt.%) alloys [9-10, 14]. After solution heat-treatment or controlled-rolling followed by an optimum aging at 550℃ for 15~16h, the UTS and YS of the FeAlMnMC (M=V, Nb, Mo, W) alloys were significantly increased up to 1130-1220 and 890-1080 MPa, respectively, with 41-26% elongation [9-10].

In our previous studies, we investigated the as-quenched microstructure of the Fe-9.8 wt.% Al -29 wt.% Mn-(1.45-2.05) wt.% C alloys, and found that an extremely high density of nano-sized κ′-carbides was formed within the γ matrix by spinodal decomposition during quenching [41]. This is quite different from that observed in the austenitic Fe-Al-Mn-C (C ≦ 1.3 wt. %) alloys, in which fine κ′-carbides could only be observed in the aged alloys. The UTS, YS and elongation of the as-quenched FeMnAlC alloys with 1.8≦C≦2.0 wt. % were 1080~1105 MPa, 868~883 MPa and 55.5~54.5 %, respectively [41-42]. Furthermore, after being aged at 450~550 ^{o}C for moderate times, the alloys could possess ultrahigh UTS ranging from 1395 to 1552 MPa and YS ranging from 1262 to 1423 MPa with a good elongation ranging from 32.5 to 25.8 % [41-42].

Although the austenitic FeMnAlMC alloys could possess excellent combination of strength and ductility, the corrosion behavior of the alloys in aqueous environments was not adequate for applications in aggressive environment [48-52]. In order to improve the corrosion resistance, Cr was added to the austenitic FeMnAlC alloys [51-54]. Consequently, it was found that the corrosion potential (Ecorr) and pitting potential (Epp) of as-quenched austenitic Fe-(29.2-31.3)wt.%Mn-(7.1-9.1)wt.%Al-(2.8-6)wt.%Cr-(0.88-1.0)wt.%C alloys in 3.5% NaCl solution were ranging from -820 to -556 mV and from -240 to -27

mV, respectively [51-54]. The results were much better than the Ecorr (-920~-789 mV) and Epp (-500~-280 mV) of the austenitic as-quenched FeMnAlC alloys [48-52].

FeMnAlC alloys could improve the corrosion resistance and maintain almost the same mechanical properties when Cr was added in FeAlMnC alloys, however, it was not a cost-effective method. Recently, nitriding was widely utilized to improve surface hardness and corrosion resistance of metallic materials. However, high strength alloy steels, martensitic as well as precipitation hardening stainless steels were needed to temper at 15 ^{o}C above the nitriding temperature prior to nitriding. These high strength alloy steels and stainless steels couldn't obtain remarkable combination of strength and ductility, as well as corrosion resistance, with the one-step treatment. It is worthwhile to explore how the corrosion behaviors and mechanical properties of the FeAlMnC alloys could be simultaneously optimized by one-step nitriding scheme for applications in aggressive environments.

Nitriding is a heat-treatment process that nitrogen diffuses into the surface of a metallic material to create a hardened surface and enhance wear resistance. It is predominantly used on alloy steels and austenitic, martensitic as well as precipitation-hardening stainless steels. The most two common methods used are: gas nitriding, and plasma nitriding. Characteristics of each method are

described as follows.

In gas nitriding the donor is a nitrogen rich gas, usually ammonia (NH_3), which is why it is sometimes known as ammonia nitriding.[57] When ammonia comes into contact with the heated work piece, it disassociates into nitrogen and hydrogen. The nitrogen then diffuses into the surface of the material creating a nitrided layer. The detailed gas nitriding process is shown in Figure 1.2.

Traditionally, gas nitriding has been used in improving wear resistance and endurance characteristics in metallic materials. The properties of a nitrided steel are determined by both the core strength and the structural characteristics of the compound layer and the diffusion zone. Recent developments have led to a process that can be accurately controlled. The thickness and phase constitution of the resulting nitrided layers can be selected and the process optimized for the particular properties required.

The gas nitriding method has advantages such as relatively low equipment cost - especially compared with plasma nitriding and all round nitriding effect.

Plasma nitriding, also known as ion nitriding, glow-discharge nitriding or plasma ion nitriding, is an industrial surface hardening treatment for metallic materials and steels. In plasma nitriding, the reactivity of the nitriding media is not due to the temperature but to the gas ionized state. In this technique intense electric fields are used to generate ionized molecules of the gas around the

surface to be nitrided. Such highly active gas with ionized molecules is called plasma, naming the technique. The gas used for plasma nitriding is usually pure nitrogen. The plasma nitriding procedure is shown in Figure 1.3.

Plasma nitriding can improve the surface hardness and wear resistance of various engineering materials, as gas nitriding. In practice, there is increasing interest by industry in plasma based nitriding technologies which offer many advantages over traditional gas nitriding, particularly, in terms of reduced gas consumption, reduced energy consumption and the completely removal of any environmental hazard. Plasma nitriding advantage is related to that not only the performance of metal parts gets enhanced but working lifespan gets boosted. Furthermore, the hardness of the surface during plasma nitriding treatment is higher than gas nitriding due to higher N concentration. Plasma nitriding can thus be performed in a broad temperature range, from 260℃ to more than 600℃. However, in conventional plasma nitriding process, the treated components are submitted to high cathodic potentials and the plasma acts directly in surface of the components. This brings some inherent shortcoming for plasma nitriding, such as damage caused to parts by arcing, the “edging effect”, and difficulty in maintaining a uniform component temperature, particularly in full workloads of components with varied dimensions and complicated shapes.

Therefore, the purpose of the present work is to investigate the microstructures, mechanical properties and corrosion behaviors of plasma-nitrided and gas-nitrided FeAlMnC alloys by using optical microscope (OM), scanning electron microscopy (SEM), transmission electron microscopy (TEM), X-ray, Glow Discharge Spectrometer (GDS) and Vicker's indenter, Potentiostat / Galvanostat and energy dispersive X-ray spectrometer (EDS) analyses. Tensile tests were carried out at room temperature with an Instron 8501 tensile testing machine at a strain rate of 6.7×10^{-4} s^{-1}. The detailed experiment results are presented in Chapters 2 and 3, recpectively.

References

[1] K. Sato, K. Tagawa, Y. Inoue, Scripta Metall. 22 (1988) 899.

[2] T.F. Liu, J.S. Chou, C.C. Wu, Metal. Trans. A 21 (1990) 1891.

[3] K.H. Han, J.C. Yoon, W.K. Choo, Scripta Metall. 20 (1986) 33.

[4] C.N. Hwang, T.F. Liu, Scripta Mater. 36 (1997) 853.

[5] C.Y. Chao, C.N. Hwang, T.F. Liu, Scripta Metall. 28 (1993) 109.

[6] K. Sato, K. Tagawa, Y. Inoue, Metal. Trans. A 21 (1990) 5.

[7] C.N. Hwang, C.Y. Chao, T.F. Liu, Scripta Metall. 28 (1993) 263.

[8] W.K. Choo, J.H. Kim, J.C. Yoon, Acta Mater. 45 (1997) 4877.

[9] I.S. Kalashnikov, O. Acselrad, A. Shalkevich, J. Mater. Process. Technol. 136 (2003) 72.

[10] G.S. Krivonogov, M.F. Alekseyenko and G.G. Solovyeva, Fiz. Metal. Metalloved 39 (1975) 775.

[11] S.C. Tjong, S.M. Zhu, Mater. Trans. 38 (1997) 112.

[12] I.S. Kalashnikov, O. Aksel'rad, M.S. Khadyev, Metal Sci. Heat Treat. 48 (2006) 5.

[13] Kalashnikov, O. Acselrad, A. Shalkevich, L.C. Pereira, J. Mater. Eng. Perform. 9 (2000) 597.

[14] I.S. Kalashnikov, B.S. Ermakov, O. Aksel'rad, L.K. Pereira, Metal Sci. Heat Treat. 43 (2001) 493.

[15] Y. Kimura, K. Handa, K. Hayashi, Y. Mishima, Intermetallics 12 (2004) 607.

[16] S.K. Banerji, Met. Prog. Apr (1978) 59.

[17] H.W. Leavenworth, Jr. and J.C. Benz, J. Met. vol. 37, (1985) 36.

[18] J. Charles, A. Berghezan, A. Lutts, P.L. Dancoisne, Met. Prog. 120 (1981) 71.

[19] R. Wang, F.H. Beck, Met. Prog. 123 (1983) 72.

[20] J.C. Garcia, N. Rosas, R.J. Rioja, Met. Prog. 124 (1982) 47.

[21] D.J. Schmatz, Trans. ASM. 52 (1960) 898.

[22] M.F. Alekseyenko, G.S. Krivonogov, L.G. Kozyreva, I.M. Kachanova, L.V. Arapova, Met. Sci. Heat Treat. 14 No.3-4 (1972) 187.

[23] L.I. Lysak, M.F. Alekseyenko, A.G. Drachinskaya, N.A. Storchak, G.S. Krivonogov, Metallofizika 59 No.4 (1975) 29.

[24] R.E. Cairns, Jr. and J.L. Ham, U.S. patent, No. 3111405 (1963).

[25] I. Briggs, G.J. Russell, A.G. Clegg, J. Mater. Sci. 20 (1985) 668.

[26] W.K. Choo, K.H. Han, Metall. Trans. A 16 (1985) 5.

[27] W.K. Choo, D.G. Kim, Metall. Trans. A 18 (1987) 759.

[28] S.C. Tjong, N.G. Ho, Metallography 21 (1988) 199.

[29] G.L. Kayak, Met. Sci. Heat Treat. 22 No.2 (1969)95.

[30] S.M. Zhu, S.C. Tjong, Metall. Trans. A 29 (1998)299.

[31] I.S. Kalashnikov, O. Acselrad, L.C. Pereira, T. Kalichak, M.S. Khadyyev, J. Mater. Eng. Perform. 9 (2000)334.

[32] S.C. Tjong, C.S. Wu, Mater. Sci. Eng. 80 (1986) 203.

[33] I.F. Tsu, T.P. Perng, Metall. Trans. A 22 (1991) 215.

[34] S.M. Zhu, S.C. Tjong, Scripta 36 (1997) 317.

[35] K. Ishida, H. Othani, N. Statoh, R. Kainuma, T. Nishizawa, ISIJ International 30 (1990) 680.

[36] C.S. Wang, C.N. Hwang, C.G. Chao, T.F. Liu, Scripta Mater. 57 (2007) 809.

[37] J.A. Sarreal, C.C. Koch, Mater. Sci. Eng. A 136 (1991) 141.

[38] J.E. Krzanowski, Metall. Trans. A 19 (1988) 1873.

[39] P.J. James, J. Iron Steel Inst. (1969) 54.

[40] K. Sato, K. Tagawa, Y. Inoue, Mater. Sci. Eng. A 111 (1989) 45.

[41] K.M. Chang, C.G. Chao, T.F. Liu, Scripta Mater. 63 (2010) 162.

[42] C.L. Lin, C.G. Chao, H.Y. Bor, T.F. Liu, Mater. Trans. 51 No.6 (2010) 1084.

[43] S.C. Tjong, N.J. Ho, Metallography 21 (1988) 1996.

[44] T.F. Liu, C.M. Wan, Strength Met. Alloys 1 (1986) 423.

[45] C.C. Wu, J.S. Chou, T.F. Liu, Metall. Trans. A 22A (1991) 2265.

[46] K.S. Chan, L.H. Chen, T.S. Lui, Mater. Trans. 38 No.5 (1997) 420.

[47] S.C. Chang, Y.H. Hsiau, M.T. Jahn, J. Mater. Sci. 24 (1989) 1117.

[48] M. Ruscak, T.P. Perng, Corrosion Oct. (1995) 738.

[49] W.T. Tsai, J.B. Duh, J.T. Lee, J. Mater. Sci. 22 (1987) 3517.

[50] J.B. Duh, W.T. Tsai, J.T. Lee, Corrosion Nov. (1988) 810.

[51] S.C. Chang, J.Y. Liu, H.K. Juang, Corrosion 51 No.5 (1995) 399.

[52] C.J. Wang, Y.C. Chang, Mater. Chem. Phys. 76 (2002) 151.

[53] C.S. Wang, C.Y. Tsai, C.G. Chao, T.F. Liu, Mater. Trans. 48 (2007) 2973.

[54] Y.H. Tuan, C.S. Wang, C.Y. Tsai, C.G. Chao, T.F. Liu, Mater. Chem. Phys. 114 (2009) 595.

[55] S.C. Chang, W.H. Weng, H.C. Chen, S.J. Lin, P.C.K. Chung, Wear 181-183 (1995) 511.

[56] S.T. Shih, C.Y. Tai, T.P. Perng, Corrosion Feb (1993) 130.

[57] Ion Nitriding and Nitrocarburizing of Sintered PM Parts, October 7, 2004

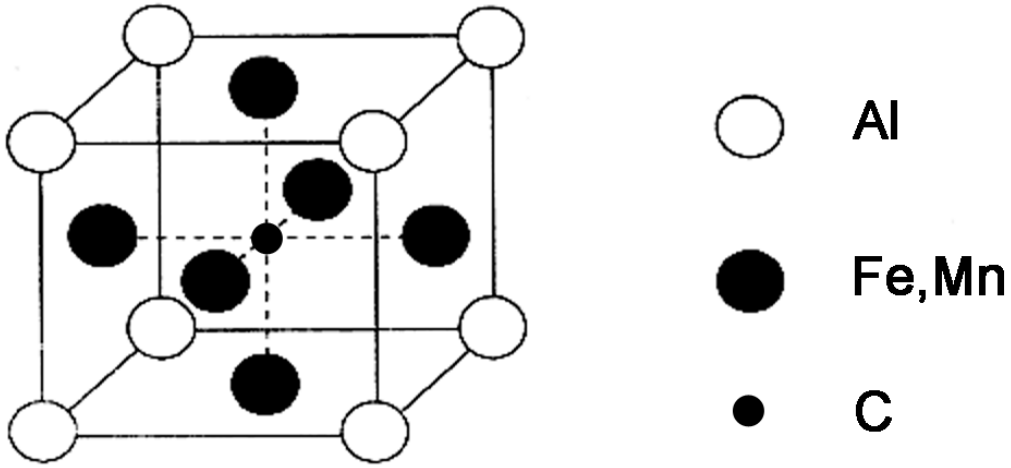

Figure 1.1(a)

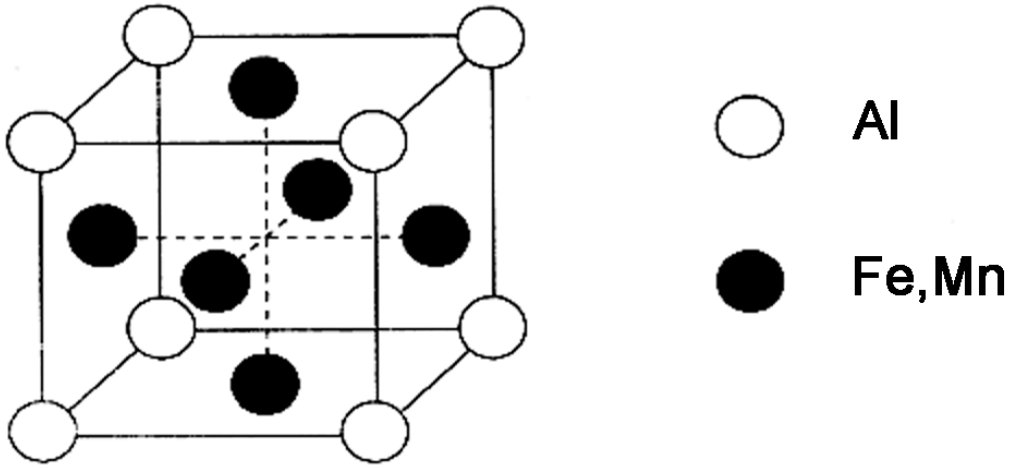

Figure 1.1(b)

Figure 1.1 (a) $L'1_2$ crystal structure. (b) $L1_2$ crystal structure.

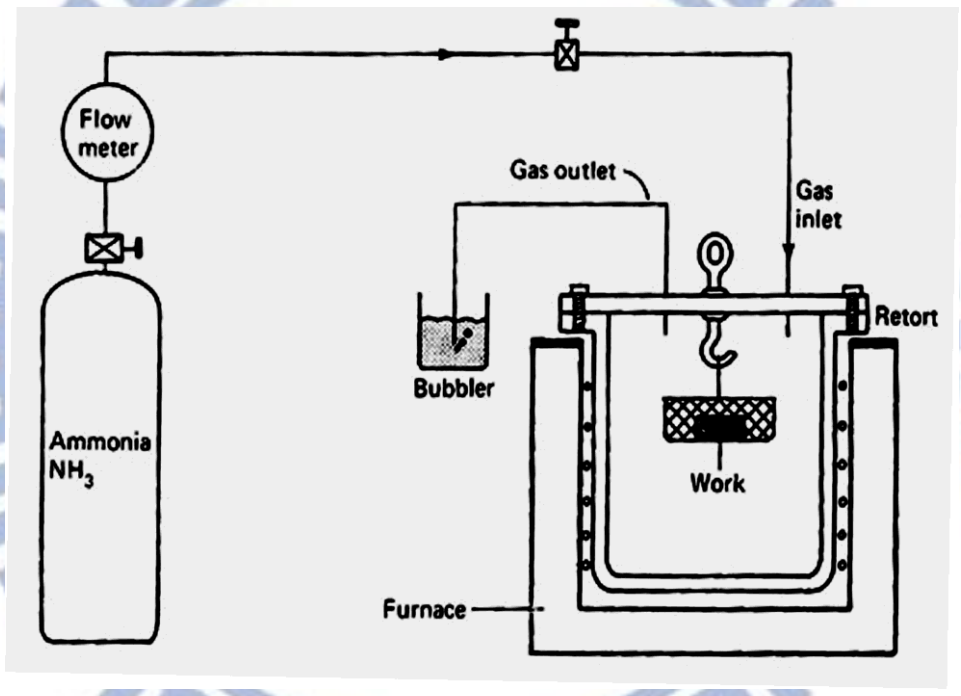

Figure 1.2 Illustration of gas nitriding

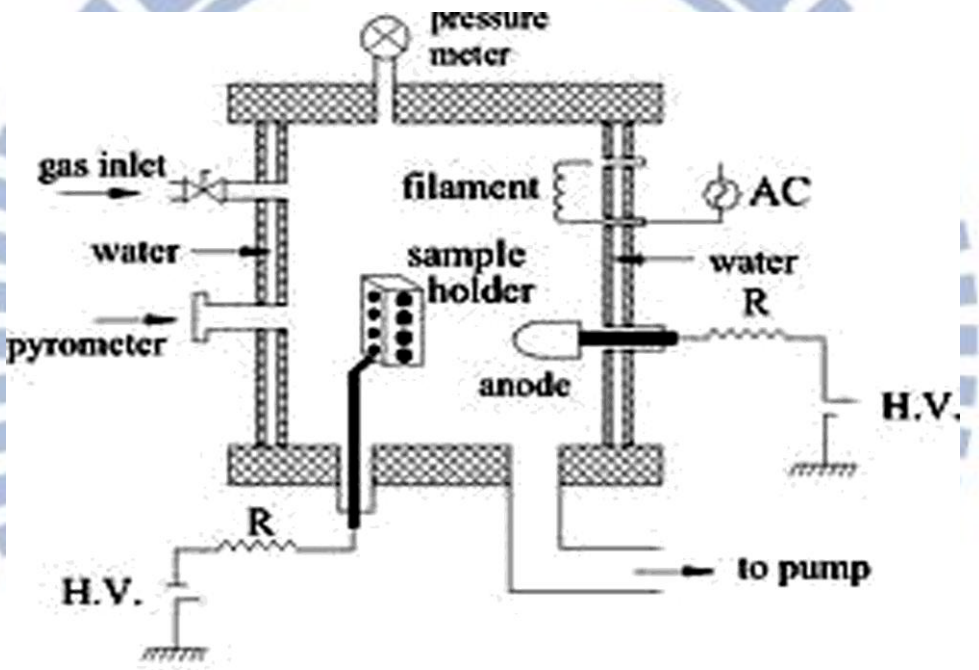

Figure 1.3 Illustration of plasma nitriding

Chapter 2.

A novel high-strength high-ductility and high corrosion-resistance FeAlMnC low-density alloy

A novel high-strength high-ductility and high corrosion-resistance FeAlMnC low-density alloy

Abstract

The as-quenched Fe-8.68 wt.% Al-30.5 wt.% Mn-1.85 wt.% C alloy is plasma nitrided at 500°C for 8h. The nitrided layer obtained is 40 μm-thick and composed predominantly of AlN with a small amount of Fe_4N. The resultant surface hardness (1860 Hv), substrate hardness (550 Hv), ductility (33.6%), and corrosion resistance in 3.5% NaCl solution in the present nitrided alloy are far superior to those obtained previously in optimally nitrided high-strength alloy steels, as well as martensitic and precipitation-hardening stainless steels.

2-1 Introduction

In view of excellent combinations of high-strength and high-ductility as well as without needing expensive strategic alloying elements (e.g. Cr, Ni, Mo), the austenitic Fe-Al-Mn-C quarternary alloys have been attracting tremendous attention. Moreover, due to high aluminum content, the density of the alloys is about 13% lower than conventional steels [1]. Previous studies showed that the as-quenched microstructure of Fe-(7.8-10) wt.% Al-(28-30) wt.% Mn-(0.8-1.3) wt.% C alloys was single-phase austenite (γ) [1-5]. An optimal combination of strength and ductility could be obtained for the Fe-Al-Mn-C alloys aged at 550^{o}C for about 16h [2, 3]. Under these aging conditions, a high density of fine $(Fe,Mn)_3AlC$ carbides (κ′-carbides) having $L'1_2$ (ordered FCC) structure precipitated coherently within γ matrix without any grain boundary precipitates. After optimal aging, the ultimate tensile strength (UTS), yield strength (YS) and elongation (El) of the Fe-Al-Mn-C alloys could reach 1130-1250 MPa, 1080-1120 MPa and 33-31%, respectively [2,3].

Recently, we investigated the as-quenched microstructure of the Fe-9.8 wt.% Al -29 wt.% Mn-(1.45-2.05) wt.% C alloys, and found that an extremely high density of nano-sized κ′-carbides was formed within γ matrix by spinodal decomposition during quenching [6]. This is quite different from that observed in the austenitic Fe-Al-Mn-C (C $\leqq$ 1.3 wt. %) alloys, in which fine κ′-carbides

could only be observed in aged alloys. Due to the pre-existing nano-sized κ′-carbides, the aging temperature and time required to attain the optimal combination of strength and ductility are, respectively, much lower and less than those of the previous Fe-Al-Mn-C (C≦1.3 wt.%) alloys. For example, with almost equivalent elongation, the Fe-9 wt. % Al -28 wt.% Mn-1.8 wt.% C alloy aged at 450°C for 12h can possess yield strength about 28% higher than that of the optimally aged Fe-Al-Mn-C (C≦1.3 wt.%) alloys [7].

Although the austenitic Fe-Al-Mn-C alloys could possess excellent combination of strength and ductility, the corrosion resistance of the alloys was insufficient for applications in aggressive environments [4,5]. Plasma nitriding was widely utilized to improve surface hardness and corrosion resistance of metallic materials [8-19]. However, to date, little information concerning the plasma nitriding treatment for Fe-Al-Mn-C alloys has been reported in the literature. The main purpose of this work is to investigate the characteristics of an Fe-8.68 wt.% Al-30.5 wt.% Mn-1.85 wt.% C alloy after plasma nitriding at 500^{o}C for 8h.

2-2 Experimental Procedure

The Fe-8.68 wt. % Al -30.5 wt.% Mn-1.85 wt.% C alloy was prepared in an air induction furnace. After being homogenized at 1150^{o}C for 6h, the ingot was hot-rolled to a 6-mm-thick plate. The plate was subsequently solution heat-treated at 1200^{o}C for 2h and then quenched into room-temperature water. The specimen was polished using SiC papers to 2400 grit before plasma nitriding. The plasma nitriding process was performed at 500^{o}C for 8h using an atmosphere of 50% N_2 and 50% H_2 under a pressure of 130Pa. Scanning electron microscopy (SEM) was used to investigate the surface and cross-sectional morphologies of the nitrided alloy by using JEOL 6500 with 15kv voltage. Transmission electron microscopy examination was performed on a JEOL JEM-2100 transmission electron microscope (TEM) operating at 200kv. TEM specimens were prepared by means of a double-jet electropolisher with an electrolyte of 60% acetic acid, 30% ethanol and 10% perchloric acid. The polishing temperature was kept in the range from -30 ^{o}C to -15 ^{o}C, and the current density was kept in the range from $3x10^{-4}$ to $4x10^{-4}$ A/m^2. X-ray diffraction (XRD) was carried out using a Bruker D8 with Cu-K_α radiation. The nitrogen concentration and microhardness of the nitrided alloy were determined by using glow discharge spectrometer (GDS) and Vicker's indenter at 100gf,

respectively. Potentiodynamic polarization curves were measured in 3.5% NaCl solution at 25^{o}C. Electrochemical polarization curves were obtained by using an EG&G Princeton Applied Research Model 273 galvanostat / potentiostat. Speciemens with an exposed surface area of ~1cm^2 were ground with 2400 grit SiC paper and then with 1.5μm Al_2O_3 powder, washed in distilled water and rinsed in acetone prior to passivation. Poteniodynamic polarization curves were obtained at a potential scan rate of 2 mV/s from -1 V to 3V. A saturated calomel electrode (SCE) and a platinum wire were used as reference and auxiliary electrodes, respectively. The specimens for tensile tests were prepared according to ASTM standards. The gauge length, width and thickness of the tensile test specimens are 50 mm, 12.5 mm and 6 mm, respectively. Tensile tests were carried out at room temperature with an Instron 8501 tensile testing machine at a strain rate of 6.7×10^{-4} s^{-1}.

2-3 Results and Discussion

Figure 2.1(a) is a TEM $(100)_{\kappa'}$ dark-field image and Figure 2.1(b)~(d) are the corresponding diffraction patterns of the as-quenched alloy, revealing that an extremely high density of nano-sized κ′-carbides can be observed within γ matrix and the nano-sized κ′-carbides were formed by spinodal decomposition during quenching [6,7]. By using a LECO 2000 image analyzer, the average size and volume fraction of the κ′-carbides were determined to be about 10 nm and 38%, respectively. A detailed investigation indicated that when the as-quenched alloy was aged at 500°C for 8h, the alloy could possess excellent combination of strength and ductility with the UTS, YS and El being 1402 MPa, 1298 MPa, and 34.5%, respectively. For achieving the effects of aging and nitriding simultaneously, the plasma nitriding was fixed at 500°C for 8h with various processing pressures and gas compositions. The experiments indicated that the working pressure of 130Pa with gas composition of 50% N_2 and 50% H_2 could give rise to the best plasma nitriding results. Figure 2.1(e) is a cross-sectional SEM image of the nitrided alloy, showing that the thickness of the nitrided layer is about 40 μm. The grain boundaries of the substrate are clearly revealed by the nital etchant, while the nitrided layer remains intact. Moreover, the boundary between nitrided layer and substrate is obscure. Figure 2.1(f) shows XRD result for the nitrided alloy, revealing that besides γ

diffraction peaks, diffraction peaks belonging to AlN and Fe_4N can also be detected. Both AlN and Fe_4N have FCC structure with lattice parameters of 4.06 nm and 3.79 nm, respectively [20,21]. Moreover, the intensity of the AlN diffraction peaks is much higher than that of Fe_4N phase, indicating that the nitrided layer is composed predominantly of AlN phase with significantly less amount of Fe_4N phase. Furthermore, the XRD peaks are fairly broadened, which may be due to the large amount of nitrogen incorporated in these phases [11-12, 15-19]. Figure 2.2(a) shows the nitrogen concentration as a function of depth, revealing that at the outmost surface, the nitrogen concentration is as high as about 20 wt.% (48 at.%). The nitrogen concentration gradually decreases with increasing depth. Figure 2.2(b) shows the microhardness of the nitrided alloy as a function of depth. The surface microhardness is extremely high (1860 Hv), and gradually decreases with increasing depth until the substrate value of about 550 Hv. Tensile test indicated that UTS, YS, and El of the nitrided alloy were 1388 MPa, 1286 MPa, and 33.6%, respectively, which are comparable to those obtained for the same alloy aged at 500^{o}C for 8h. By slightly tilting the specimen, the fracture and free surfaces could be observed simultaneously, as illustrated in Figure 2.2(c). High density of dimples can be seen within the austenite + κ′-carbides matrix, and no microvoids or microcracks are observed in the vicinity of the interface between nitrided layer

and substrate. Obviously, the substrate remains ductile and the nitrided layer itself is very compact with good adhesion to the substrate.

Potentiodynamic polarization curves for as-quenched and plasma nitrided alloys in 3.5% NaCl solution are shown in Figure 2.3(a). Evidently, for the untreated alloy (curve I), there is no apparent passivation region. The corrosion current density (i_{corr}) and corrosion potential (E_{corr}) are 2×10^{-6} A/cm^2 and -790 mV, respectively. However, an obvious passivation region can be observed for the nitrided alloy (curve II), and i_{corr} is evidently reduced by about three orders of magnitude to 6×10^{-10} A/cm^2 and E_{corr} is drastically improved to +50 mV. Moreover, the values of the pitting corrosion current density (i_p) and pitting potential (E_{pit}) for the nitrided alloy are 2×10^{-7} A/cm^2 and +2030 mV, respectively. Apparently, plasma nitriding has resulted in a pronounced enhancement in corrosion resistance. Figures 2.3(b) and 2.3(c) are SEM images of the corroded surfaces, indicating that during polarization the grain boundaries and γ matrix of the untreated alloy were severely attacked, while only a few very small (~0.3 μm) corrosion pits (as indicated with arrows in Figure 2.3(c)) were formed for the nitrided alloy.

That the nitrided layer of the present nitrided alloy is composed predominantly AlN with a small amount of Fe_4N is a remarkable feature. For many industrial applications requiring high strength, high wear resistance and

high corrosion resistance, the nitrided low-Cr (Cr＜1.2 wt.%) alloy steels (e.g. AISI 4140, 4340 and 5140) and high-Cr (Cr＞12 wt.%) martensitic stainless steels (e.g. AISI 410) as well as precipitation-hardening (PH) stainless steels(e.g. AISI 17-4PH) were widely used. According to extensive previous studies, the optimal nitriding conditions for the low-Cr steels were 520-550 ^{o}C for 4-6h [8-10], while those for high-Cr stainless steels were 400-480 ^{o}C for 2-20h [11-19]. The nitrided layer formed in these body-centered cubic (BCC) steels is mainly composed of Fe_3N (HCP) and Fe_4N (FCC), without or with a trace of CrN (FCC) [8-19]. After optimal nitriding treatment, the surface microhardness of the low-Cr alloy steels and high-Cr stainless steels were between 890-940 Hv and 1000-1350 Hv, respectively, which are far lower than 1860 Hv obtained in the present nitrided alloy. The primary reason is that due to AlN formation in the present nitrided alloy, nitrogen concentration near the surface can reach 20 wt.%; whereas the surface nitrogen concentrations of the optimally nitrided low-Cr alloy steels and high-Cr stainless steels were 5.7-10 wt.% and 10-15 wt.%, respectively [17,22-25]. The hardness of the nitrides generally increases with increasing nitrogen concentration. For instance, the hardness of AlN is 25.7GPa [26], which is much higher than that of Fe_3N (11.2-12.4 GPa), and Fe_4N (8.6-11.2 GPa) [22, 27]. It is worthwhile to emphasize here that the substrate hardness (550Hv) of the present nitrided

alloy is also much higher than 210-400 Hv obtained in the optimally nitrided high-strength alloy steels and stainless steels [9-16, 18]. The reason is that prior to nitriding, these steels need to temper at 15°C above the nitriding temperature [28], and then nitrided at the optimal temperature for a long duration. This would deteriorate the substrate hardness drastically [23]. Detailed comparisons of surface hardness and substrate hardness are listed in Table 1.

The most important indicators for evaluating the corrosion resistance of metallic materials are i_{corr}, i_p, E_{corr}, and E_{pit}; lower current densities and higher potentials indicate better corrosion resistance [8-19]. Table 1 lists the values of i_{corr}, i_p, E_{corr}, and E_{pit} obtained using the same SCE in 3.5% NaCl solution at room-temperature for the present nitrided alloy, and the previous results for the optimally nitrided low-Cr alloy steels (including 4140, 4340, and 5140), high-Cr 410 martensitic stainless steels, 17-4 precipitation hardening steels (17-4PH) and austenitic stainless steels (including AISI 304, 316). In Table 1, it is obvious that the corrosion resistance of the present nitrided alloy is far superior to that of the low-Cr alloy steels and high-Cr stainless steels. The reasons are described in detail as follows. It is indicated that the low-Cr alloy steels have the lowest surface and substrate hardness. The reason is that prior to nitriding, these steels need to temper at 15°C above the nitriding temperature, and then nitrided at the optimal temperature for a long duration. This would

deteriorate the substrate hardness drastically. Moreover, it has shown that plasma nitriding is effective in improving the tribological properties and surface hardness of 410 and 420 martensitic stainless steels under various testing conditions [11-12]. It is also indicated that when nitriding is carried out below a temperature at which CrN forms, the nitrided layer retains its martensite structure but with a larger lattice parameter than the bulk, so that "expanded martensite" has been proposed in comparison to "expanded austenite". For this reason, surface hardness of the optimally nitrided martensite stainless steels is slightly lower than that of austenitic stainless steels. Additionally, 17-4PH stainless steels have been widely utilized in industries. However, nitrided 17-4PH stainless steel has low surface hardness and poor tribological properties, which could limit its applications in such areas where contact and wear are involved. Some surface modification methods have been carried out for improving the properties of this kind of steel. Recently, plasma nitriding treatments on 17-4PH steel at lower temperature have been developed. It indicates that these treatments can provide a considerable improvement in the wear resistance of the precipitation-hardening stainless steels without significantly compromising its desirable corrosion-resistant properties. Consequently, 17-4PH steel also has the excellent combination of surface hardness and corrosion resistance. Finally, it is clearly shown that austenite

stainless steels have the highest surface hardness than other low-Cr and high-Cr steels. It has been explained that when nitriding temperature is sufficiently low, a nitrogen expanded austenite (namely S-phase) can be produced on the surface of the austenite stainless steel. Due to contain a significant amount of nitrogen in the S-phase, the low temperature nitrided austenitic stainless steels can possess not only considerably increased surface hardness and wear resistance, but also much improved corrosion resistance. For example, when nitriding at a temperature around or below 500^{o}C can produce a thick nitrided case on the austenitic stainless steels surface, which indeed largely improve the surface hardness and wear resistance [15-19]. However, corrosion resistance of the austenitic stainless steels is dramatically reduced after nitriding at higher temperature due to the formation of chromium nitride and the depletion of free chromium in the austenite matrix. Consequently, the higher temperature nitrided stainless steel is thus no longer stainless.

Evidently, under the same testing conditions, the i_{corr} and i_{p} of the present alloy are two or three orders of magnitude lower, while the values of E_{corr} and E_{pit} are significantly higher than those of the alloy steels and stainless steels, indicating that the present nitrided alloy has far superior corrosion resistance in 3.5 % NaCl solution. Moreover, the size of the surface corrosion pits of the present nitrided alloy is only about 0.3 μm (Figure 2.3(c)), which is much

smaller than that (10-200 μm) observed in optimally nitrided alloy steels and stainless steels under similar polarization tests [8-9,12-14]. The lower i_p value results in smaller corrosion pits [12, 14], which is in good agreement with the experimental results shown in Table 1. Another important criterion for evaluating the pitting resistance is the difference between E_{pit} and E_{corr}, namely $\Delta E = E_{pit} - E_{corr}$ [29]. In Table 1, the ΔE value for optimally nitrided alloy steels and stainless steels is between +270 ~ +1330 mV, while that for the present nitrided alloy is +1980 mV, which again demonstrates the superior characteristics of the present nitrided alloy, presumably due to the high nitrogen concentration at surface [17].

Another feature of the present study is that after etching the boundary between nitrided layer and substrate was obscure (Figure 2.1(e)) and no microvoids or cracks could be detected between nitrided layer and substrate of the fractured surface (Figure 2.2(c)). This is attributed to the fact that both AlN and Fe_4N phases have the same FCC crystal structure as the γ matrix and κ′-carbides with very similar lattice parameters, which may result in excellent adhesion between nitrided layer and substrate.

2-4 Conclusions

The as-quenched microstructure of the present alloy is ductile γ phase containing an extremely high density of nano-sized κ′-carbides formed through spinodal decomposition during quenching. The as-quenched alloy is plasma nitrided at 500°C for 8h resulting in the effects of aging and nitriding simultaneously. Furthermore, the resultant 40 μm-thick nitrided layer is composed predominantly of AlN, the nitrogen concentration at surface is extremely high up to 20 wt.%. Consequently, the surface microhardness (1860 Hv), substrate hardness (550 Hv), ductility (33.6%) and corrosion resistance in 3.5% NaCl solution of the present nitrided alloy are far superior to those obtained previously for the optimally nitrided high-strength alloy steels as well as martensitic and precipitation-hardening stainless steels.

References

[1] G.S. Krivonogov, M.F. Alekseyenko, G.G. Solov'yeva: Fitz. Metal. Metalloved 39 (1975) 775.

[2] W.K. Choo, J.H. Kim, J.C. Yoon, Acta Mater. 45 (1997) 4877.

[3] I. Kalashnikov, O. Acselrad, A. Shalkevich, L.C. Pereira, J. Mater. Eng. Perform. 9 (2000) 597.

[4] Y.H. Tuan, C.S. Wang, C.Y. Tsai, C.G, Chao, T.F. Liu, Mater. Chem. Phys. 114 (2009) 595.

[5] M. Ruscak, T.P. Perng, Corrosion October (1995) 738.

[6] G.D. Tsay, Y.H. Tuan, C.L. Lin, C.G. Chao, T.F. Liu, Mater. Trans. 52 (2011) 521.

[7] K.M. Chang, C.G. Chao, T.F. Liu, Scripta Mater. 63 (2010) 162.

[8] Y. Li, L. Wang, D. Zhang, L. Shen, Applied Surface Science, 256 (2010) 4149.

[9] T. Savisalo, D.B. Lewis, Q. Luo, M. Bolton, P. Hovsepian, Surf. Coat. Technol. 202 (2008) 1661

[10] Y. Li, L. Wang, D. Zhang, L. Shen, J. Alloys. Compd. 497 (2010) 285.

[11] P. Corengia, G. Ybarra, C. Moina, A. Cabo, E. Broitman, Surf. Coat. Technol. 187 (2004) 63.

[12] C.X. Li, T. Bell, Corrosion Science 48 (2006) 2036.

[13] R.F. Liu, M.F. Yan, Mater Des 31 (2010) 2355.

[14] R.F. Liu, M.F. Yan, Surf. Coat. Technol. 204 (2010) 2251.

[15] W. Liang, Applied Surface Science 211 (2003) 308.

[16] L. Shen, L. Wang, Y. Wang, C. Wang, Surf. Coat. Technol. 204 (2010) 3222.

[17] C.X. Li, T. Bell, Corrosion Science 46 (2004) 1527.

[18] H.R. Abedi, M. Salehi, Mater Des 32 (2011) 2100.

[19] M. Olzon-Dionysio, S.D. de Souza, R.L.O. Basso, S. de Souza, Surf. Coat. Technol. 202 (2008) 3607.

[20] S.H. Sheng, R.F. Zhang, S. Veprek, Acta Materia. 56 (2008) 968.

[21] Y. Utsushikawa, K. Niizuma, J. Alloys. Compd. 222 (1995) 188.

[22] H.A. Wriedt, N.A. Gokcen, R.H. Nafziger, Bull. Alloy Phase Diagram 8 (1987)355

[23] W.P. Tong, N.R. Tao, Z.B. Wang, J. Lu, K. Lu, Science 299 (2003) 686.

[24] G.J. Li, J. Wang, Q. Peng, C. Li, Y. Wang, B.L. Shen, J. Mater. Proc. Technol. 207 (2008) 187.

[25] G.J. Li, J. Wang, C. Li, Q. Peng, J. Gao, B.L. Shen, Nucl. Instr. and Meth. B 266 (2008) 1964.

[26] J.K. Park, Y.J. Baik, Materials Letters 62 (2008) 2528.

[27] E.A. Ochoa, C.A. Figueroa, F. Alvarez, Surf. Coat. Technol. 200 (2005)

2165.

[28] W.H. Cubberly, V. Masseria, C.W. Kirkpatrick, B. Sanders, Metal Handbook V.4 Heat Treating, ninth ed., American Society for Metals, Park, Ohio 44073

[29] A. Neville, T. Hodgkiess, Corrosion Science 38 (1996) 927.

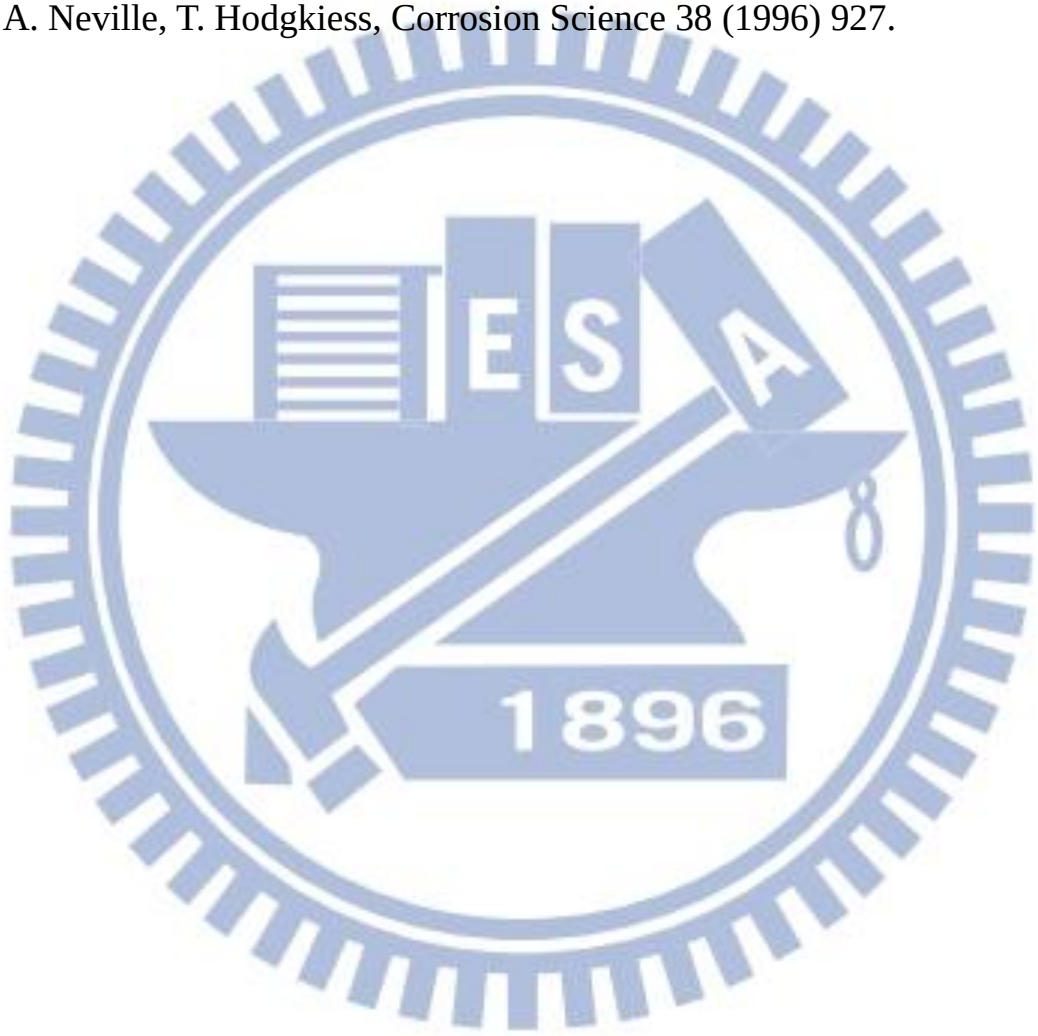

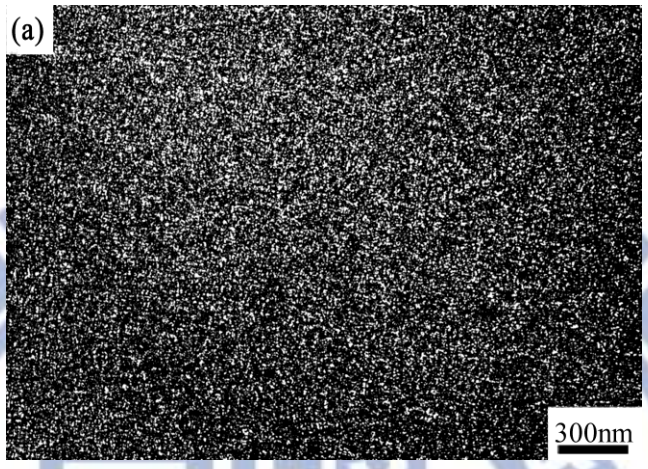

Figure 2.1(a)

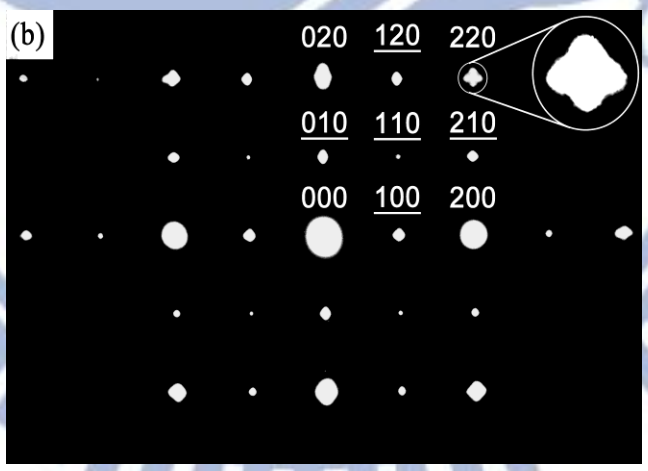

Figure 2.1(b)

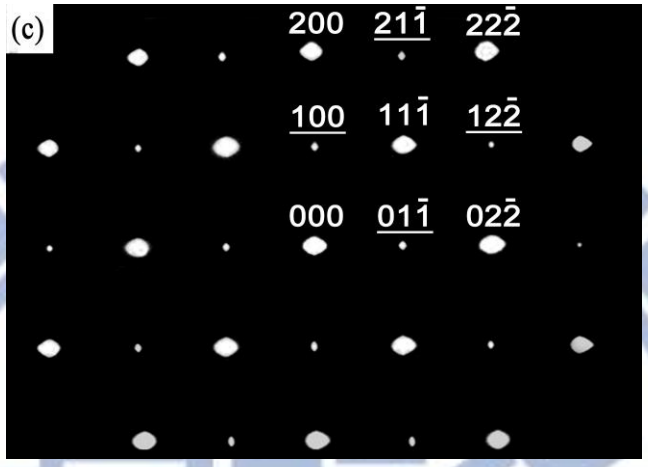

Figure 2.1(c)

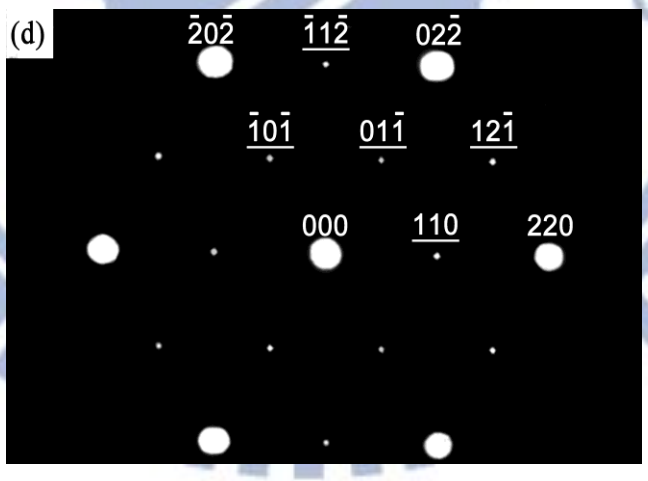

Figure 2.1(d)

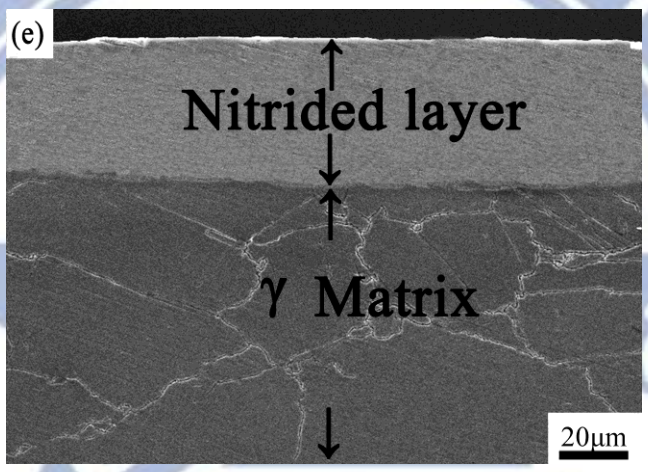

Figure 2.1(e)

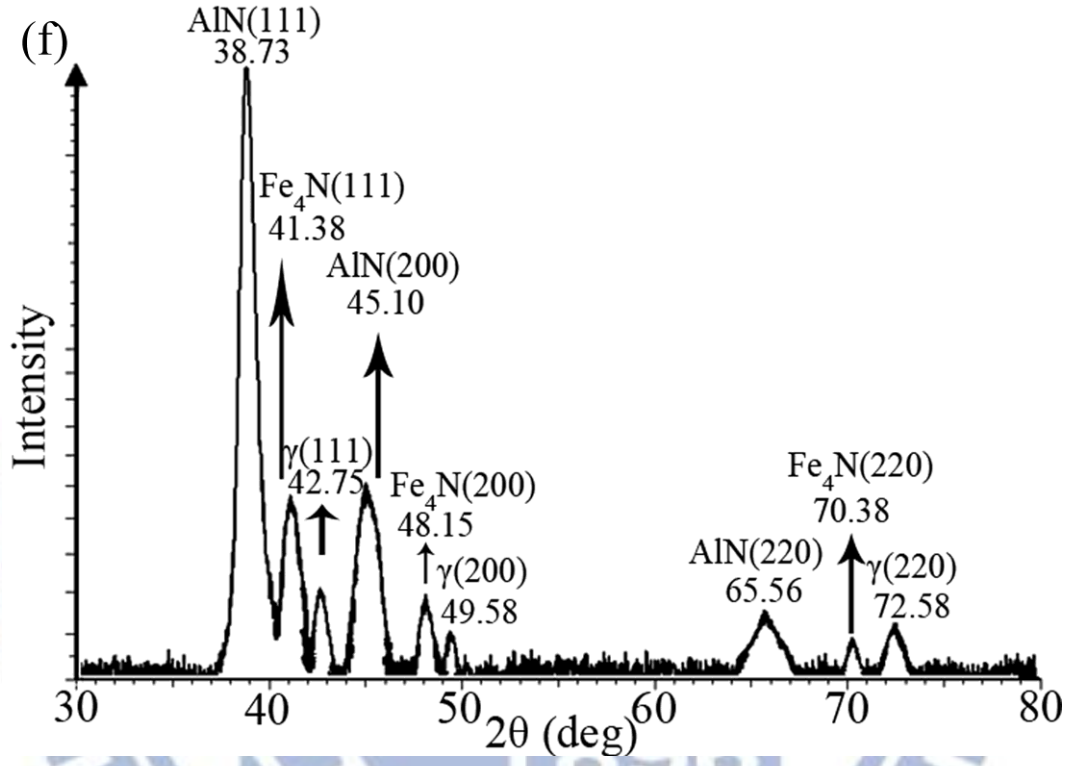

Figure 2.1(f)

Figure 2.1 (a)TEM $(100)_{\kappa'}$ dark-field (DF)image of the as-quenched alloy. (b)~(d)The selected area diffraction patterns (SADPs) taken from the as-quenched alloy (hkl:γ, <u>hkl</u>: κ′-carbide). The zone axis are [001], [011] and [$\bar{1}$11], respectively. (e) SEM image of the present nitrided alloy (etched in 5% nital). (f) X-ray diffraction pattern for the present nitrided alloy.

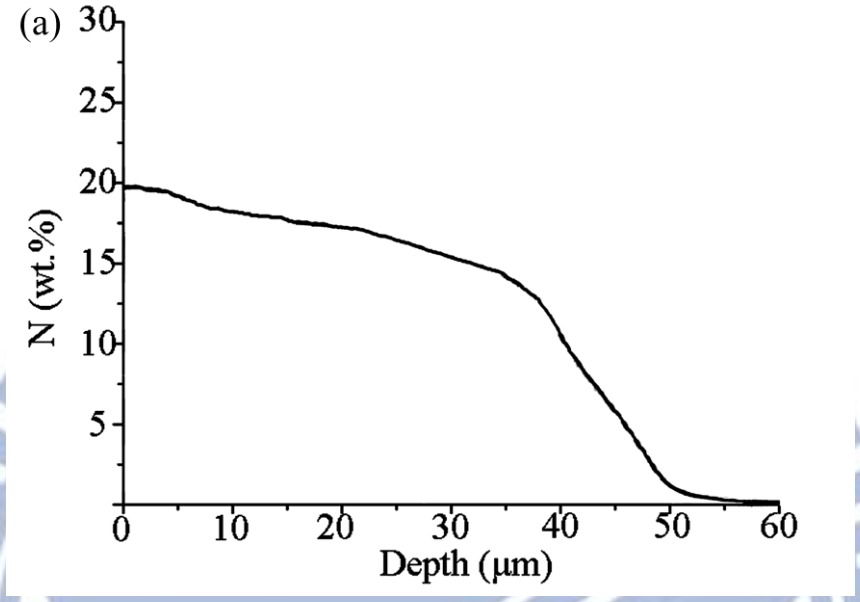

Figure 2.2(a)

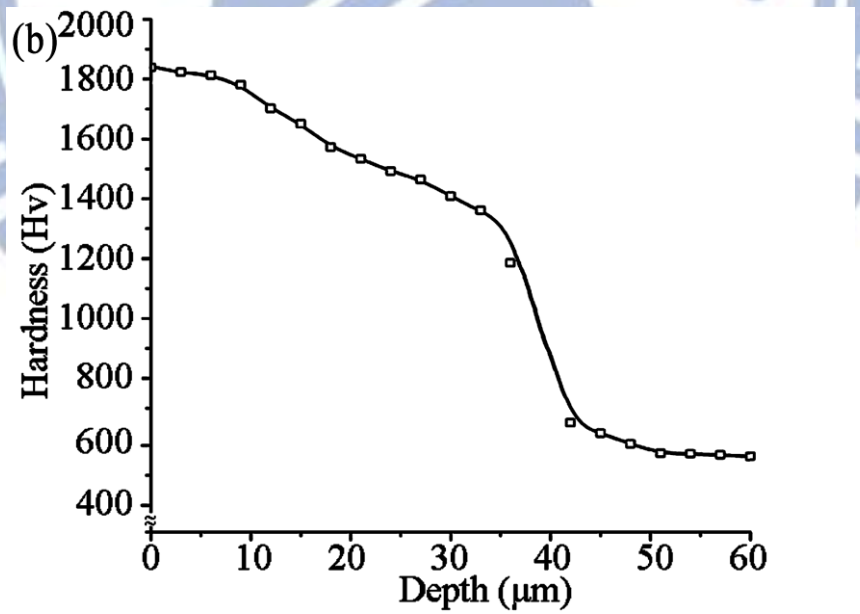

Figure 2.2(b)

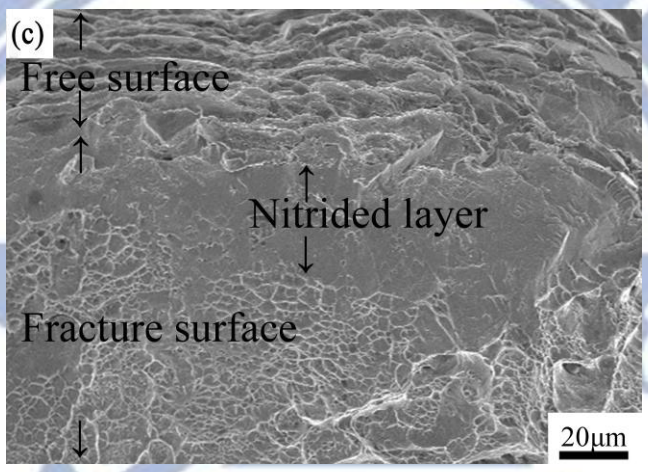

Figure 2.2(c)

Figure 2.2 (a)Nitrogen concentration profile measured by GDS of the present nitrided alloy. (b)Hardness profile of the present nitrided alloy. (c) SEM image of the present nitrided alloy after tensile test.

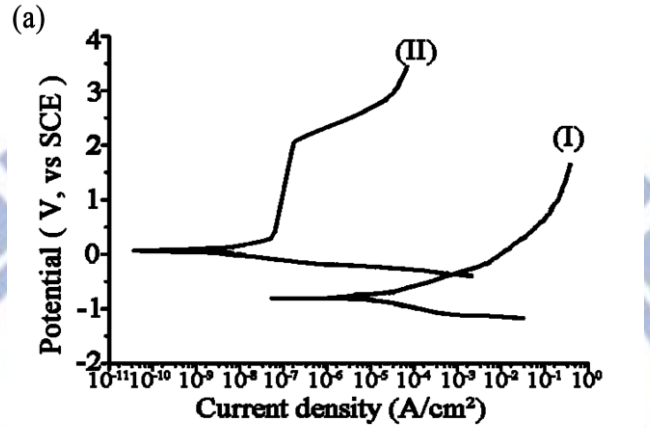

Figure 2.3(a)

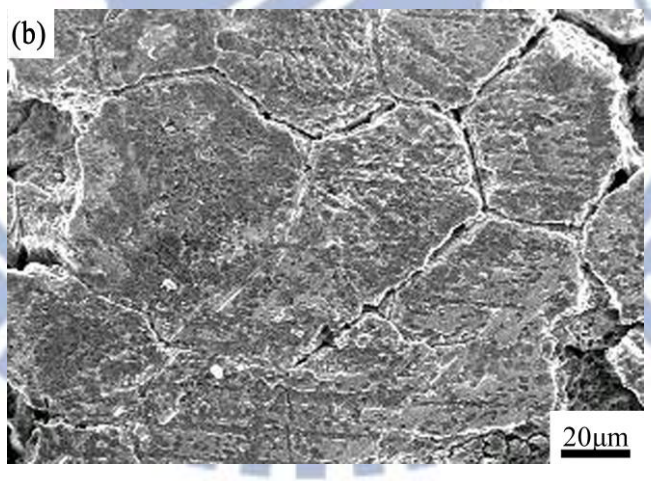

Figure 2.3(b)

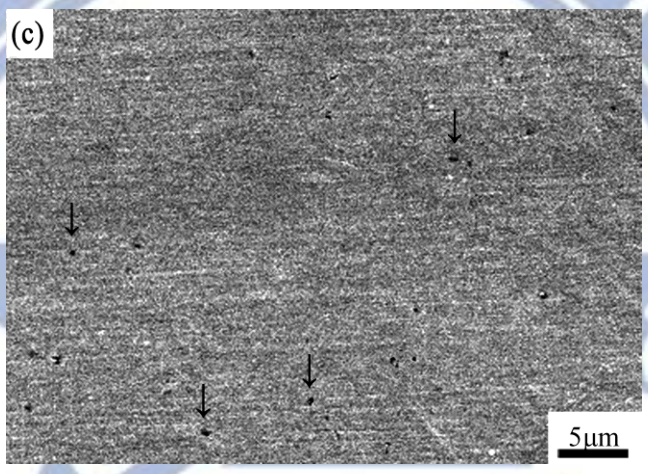

Figure 2.3(c)

Figure 2.3 (a)Polarization curves for the present untreated and nitrided alloys in 3.5% NaCl solution. (b)-(c) SEM images of the corroded surfaces for the present untreated and nitrided alloys, respectively.

Alloy	Polarization test results in 3.5% NaCl solution					Hardness (Hv)	
	I_{corr} (A/cm^2)	I_p (A/cm^2)	E_{corr} (mV)	E_{pit} (mV)	△E (mV)	surface	substrate
Alloy Steels	$8x10^{-8}$~$4x10^{-7}$	$4x10^{-6}$~$9x10^{-6}$	-400~-200	+500~+800	+770~+1000	890~940	275~320
410 (MSS)	$6x10^{-8}$~$6x10^{-7}$	$8x10^{-5}$~$8x10^{-4}$	-220~-30	+50~+600	+270~+630	1150~1204	210~262
17-4PH(SS)	$4.1x10^{-6}$~$9x10^{-6}$	$9x10^{-6}$~$1.3x10^{-5}$	-208~-207	+700~+715	+907~+923	1160~1167	360~400
304 (SS)	$1.46x10^{-8}$~$1x10^{-7}$	$4x10^{-7}$~$2x10^{-6}$	-300~-98	+125~+400	+425~+498	1000~1200	220~250
316 (SS)	$1x10^{-7}$~$3.5x10^{-7}$	$1x10^{-5}$~$8x10^{-5}$	-330~-83.8	+600~+1200	+683.8~+133	1350	220
Present Alloy	$6x10^{-10}$	$2x10^{-7}$	+50	+2030	+1980	1860	550

Table 2.1 Comparisons of polarization test results in 3.5% NaCl solution and hardness of the plasma nitrided Fe-8.68wt.%Al-30.5wt.%Mn-1.85 wt.%C alloy and the optimally plasma nitrided alloy steels as well as various stainless steels.

Chapter 3.

Structure and properties of gas-nitrided nanostructured Fe-9wt.%Al-28wt.%Mn-1.8wt.%C alloy

Structure and properties of gas-nitrided nanostructured Fe-9wt.%Al-28wt.%Mn-1.8wt.%C alloy

Abstract

The as-quenched Fe-9wt.%Al-28wt.%Mn-1.8wt.%C alloy was directly gas-nitrided at 500°C for 8h, resulting in a ~30 μm-thick nitrided layer. The nitrided layer consists predominantly of nano-crystalline AlN with a small amount of Fe_4N. The nitrogen concentration at surface was extremely high up to ~17 wt.% (~41 at.%) . Consequently, the surface microhardness (1700Hv), substrate hardness (550Hv), ductility (33.2%) and corrosion resistance in 3.5% NaCl solution of the present gas-nitrided alloy are far superior to those obtained previously for the optimally gas-nitrided or plasma-nitrided high-strength alloy steels, as well as martensitic and precipitation-hardening stainless steels. Moreover, it is very novel that the nitrided layer almost remained coherent and adhered well with the matrix after tensile test. Additionally, the present gas nitriding appeared to overcome the edge effects commonly encountered in plasma nitriding treatments for metals.

3-1 Introduction

The austenitic Fe-Al-Mn-C quarternary alloys having an excellent combination of strength and ductility, are promising materials for a wide variety of lightweight structural applications. Previously, we reported that the as-quenched microstructure of the Fe-9wt.%Al-28wt.%Mn-1.8wt.%C alloy was single-phase austenite (γ) containing an extremely high density of nano-sized κ′-carbides formed within γ-matrix by spinodal decomposition during quenching [1]. Due to the pre-existing nano-sized κ′-carbides, the aging time required for attaining the optimal combination of strength and ductility was much less that of the previous Fe-Al-Mn-C with C≦1.3 alloys [1-3]. Additionally, with almost equivalent elongation, the alloy aged at 450°C for 12h can possess yield strength about 28% higher than that of the optimally aged Fe-Al-Mn-C with C≦1.3 alloys. Recently, in order to simultaneously harvest the excellent combination of strength and ductility as well as good corrosion resistance for applications in aggressive environments, plasma nitriding was carried out on a Fe-8.68wt.%Al-30.5wt.%Mn-1.85wt.%C alloy at 500^{o}C for 8h [4]. Consequently, unprecedented results of the surface microhardness (1860 H_V), substrate hardness (550 Hv), ductility (33.6%) and pitting potential in 3.5% NaCl solution (+2030 mV) were obtained [4]. However, since plasma nitriding is susceptible to generate a negative glow zone of plasma discharge induced by

the edge effect, it is generally unfavorable for components with sharp edges or complicated shapes [5-6]. In this respect, gas nitriding processes not only are characterized by relatively low cost and comparatively higher ecological safety, but also are more thermodynamically stable with more predictable conditions [7-8], thus are suitable for treating components of virtually any size and shape. To the best of our knowledge, little information is available concerning gas nitriding of Fe-Al-Mn-C alloys. Therefore, the aim of this work is to investigate the characteristics of gas-nitrided Fe-9wt.%Al-28wt.%Mn-1.8wt.%C alloy.

3-2 Experimental Procedure

The Fe-9wt.%Al-28wt.%Mn-1.8wt.%C alloy was prepared in an air induction furnace. After being homogenized at 1150^{o}C for 6h, the ingot was hot-rolled to a 6-mm-thick plate. The plate was subsequently solution heat-treated at 1200^{o}C for 2h and then quenched into room-temperature water. The specimen was polished using SiC papers to 2400-grit before gas nitriding. The gas nitriding process was performed at 500°C for 8h using an atmosphere of 50% NH_3 and 50% H_2. Scanning electron microscopy (SEM) was used to investigate the surface and cross-sectional morphologies of the nitrided alloy before and after tensile test. X-ray diffraction (XRD) was carried out using a Bruker D8 with Cu-Kα radiation (λ =0.154nm). The nitrogen concentration and microhardness of the nitrided alloy were determined by using glow discharge spectrometer (GDS) and Vicker's indenter at 100gf, respectively. Potentiodynamic polarization curves were measured in 3.5% NaCl solution at 25^{o}C. Electrochemical polarization curves were obtained by using an EG&G Princeton Applied Research Model 273 galvanostat / potentiostat. Speciemens with an exposed surface area of ~1cm^2 were ground with 2400-grit SiC paper and then with 1.5μm Al_2O_3 powder, washed in distilled water and rinsed in acetone prior to passivation. Poteniodynamic polarization curves were obtained at a potential scan rate of 2 mV/s from -1 V to 3V. A saturated calomel electrode

(SCE) and a platinum wire were used as reference and auxiliary electrodes, respectively. The specimens for tensile tests were prepared according to ASTM standards. The gauge length, width and thickness of the tensile test specimens are 50 mm, 12.5 mm and 6 mm, respectively. Tensile tests were carried out at room temperature with an Instron 8501 tensile testing machine at a strain rate of 6.7×10^{-4} s^{-1}.

3-3 Results and Discussion

Figure 3.1(a) is the cross-sectional SEM image of the present gas-nitrided alloy, revealing that the nitrided layer is ~30 μm-thick with the top-most 2 μm exhibiting very white appearance. It is noteworthy that the thickness of the present gas-nitrided layer is thinner than that obtained in previous plasma-nitrided alloy (~ 40μm) [4]. It has been well-established that when performing gas and plasma nitriding, respectively, on alloys containing nitride-forming elements (e.g. Al, Cr) under the same treatment conditions (i.e. same time and temperature), the nitrided layer obtained in plasma nitriding was always thicker than in gas nitriding; whereas the reverse result was obtained for alloys without nitride-forming elements [9]. The inset image in Figure 3.1(a) is an enlarged microstructure contiguous to interface between the nitrided layer and γ matrix. The average size of κ′-carbides has increased to ~25 nm, which is similar to what is expected for attaining optimal combination of mechanical properties for the Fe-8.68wt.%Al-30.5wt.%Mn-1.85wt.%C alloy [4]. Indeed, the ultimate tensile stress (UTS), yield strength (YS), and elongation (El) of the present gas-nitrided alloy are 1390 MPa, 1292 MPa, and 33.2%, respectively, The results are comparable to those obtained for the same alloy after being plasma nitrided at 500°C for 8h (1402 MPa, 1298 MPa, and 34.5%)[4]. Figures 3.1(b) through Figure 3.1(e) show the elemental mapping in the rectangular

region marked in Figure 3.1(a). The results clearly delineate that Al has diffused outward and accumulated in the vicinity of surface to interact with inward-diffusing N. On the contrary, the concentrations of Fe and Mn in the nitrided layer appear to be less than those in the γ -matrix. The XRD results shown in Figure 3.1(f) reveal that the nitrided layer is composed predominantly of nano-crystalline AlN (5~10 nm) with a small amount of Fe_4N. Moreover, the diffraction peaks of the γ-phase appear to be significantly broadened and shift to the lower diffraction angles, indicative of strained and expanded lattice arising from nitrogen incorporation [10]. This is similar to that observed previously in plasma nitriding of the same alloy [4].

Figure 3.2(a) shows the depth-dependence of microhardness of the present gas-nitrided alloy. It is clearly shown that the surface hardness can reach 1700 Hv and gradually decreases with the depth. Figure 3.2(b) shows the depth-dependence of nitrogen concentration of the gas-nitrided alloy. The nitrogen concentration at the surface is about 17 wt. % (~41 at. %), and exhibits an apparent plateau within the first several μm. Potentiodynamic polarization curves for the as-quenched and gas-nitrided alloys in 3.5% NaCl solution is shown in Figure 3.2(c). Evidently, for the untreated alloy, there is no apparent passivation region. The corrosion current density (i_{corr})and corrosion potential (E_{corr}) are 2×10^{-6} A/cm^2 and -790 mV, respectively The corrosion

current density (I_{corr}), corrosion potential (E_{corr}), pitting corrosion current density (I_p), pitting potential (E_{pit}) and Δ E(E_{pit} — E_{corr}) were measured to be 5×10^{-6} A-cm^{-2}, +25 mV, 9×10^{-9} A-cm^{-2}, +25 mV and +1710mV, respectively. Evidently, the surface microhardness and corrosion resistance behavior of the gas-nitrided alloy are slightly lower than those obtained by plasma nitriding [4]. The slight differences in surface hardness and corrosion resistance are due to the differences in thickness and compositions of the nitrided layer. Nevertheless, we emphasize here that such values of microhardness and corrosion resistance are still far superior to those obtained in optimally nitrided high-strength alloy steels, martensitic and precipitation-hardening stainless steels [4, 10-12]; In these high-strength body-centered cubic (B.C.C.) steels, the nitrided layer is mainly composed of Fe_3N (hexagonal close packed, hcp) and Fe_4N (fcc), without or with a trace of CrN (fcc), and the surface nitrogen concentration is in the range of 10~15 wt.% [13-15]. It is known that higher nitrogen concentration and dense packing of finer nitride particles can considerably improve the surface hardness and corrosion resistance of the nitrided alloys [13-15]. Figure 3.2(d) clearly indicates that the surface of the nitrided layer consists of very dense and extremely fine AlN nitride particles, which combining with the high nitrogen concentration near the surface thus explained the excellent properties of the present gas-nitrided alloy.

Next we will discuss the fracture behaviors of the nitrided layer, which have been largely ignored, despite that both gas and plasma nitriding have been ubiquitously applied to metal alloys, for improving surface microhardness and corrosion resistance. Figure 3.3(a) is a SEM image taken from the free surface of the nitrided-alloy after tensile test. There are several salient features to be noted: (1) the nitrided layer deforms commensurately with the underneath γ-matrix along the direction of applied stress; (2) the top-most nitrided layer fractures evenly with cracks running perpendicular to the stress direction; (3) the fractured fragments do not spall and detach from the substrate; (4) the fractured layer is ~1.7 μm-deep (AFM image in Figure 3.3(b)), which is consistent with the thickness of the white thin layer seen in Figure 3.1(a); (5) the wavy morphology of the fractured layer also suggests that even AlN layer is not completely brittle, presumably due to the uniform nano-sized microstructure and/or substantial nitrogen concentration existing in this layer is less than that of the stoichiometric AlN (N~50 at.%). Moreover, the tilted SEM image shown in Figure 3.3(b) revealing simultaneously the free and fracture surfaces indicates that there are high density of dimples existing within the γ+κ′-carbides matrix, while no microvoids or microcracks can be observed in the vicinity of the interface, albeit the fracture surface of the nitrided layer does not contain as many dimples typical for ductile deformation. The coherent

deformation and excellent adhesion between the nitrided layer and substrate may be attributed to the fact that AlN, Fe_4N, γ-matrix and κ′-carbides all are having the same fcc crystal structure with very similar lattice parameters [4]. Finally, we turn to the edge effect on gas nitriding process. Figure 3.4 shows a typical gas-nitrided layer around a sharp sample corner. Clearly, the thickness of the nitrided layer around the corner is thicker than that of the nearby straight regions, which is in contrast to what is usually seen in plasma nitriding [6], suggesting that gas nitriding maybe more favorable for processing components with sharp edges and complicated shapes.

3-4 Conclusions

Due to contain high content of strong nitride-forming element Al, the nitrided layer consists predominantly of nano-crystalline AlN with a small amount of Fe_4N in the present Fe-9wt.%Al-28wt.%Mn-1.8wt.%C alloy after being gas-nitrided at 500°C for 8h, The resultant nitrided layer accounts for the large surface microhardness (~1700 Hv), and the superior corrosion resistance in 3.5% NaCl solution, as well as the coherent and adhesive fracture behavior obtained. Moreover, gas nitriding appears to yield more uniform nitrided layer without suffering the edge effects.

References

[1] K.M. Chang, C.G. Chao, T.F. Liu, Scripta Mater. 63 (2010) 162.

[2] W.K. Choo, J.H. Kim, J.C. Yoon, Acta Mater. 45 (1997) 4877.

[3] I. Kalashnikov, O. Acselrad, A. Shalkevich, L.C. Pereira, J. Mater. Eng. Perform. 9 (2000) 597.

[4] P.C. Chen, C. G. Chao, T.F. Liu, Scripta Mater. 68 (2013) 380.

[5] P. Kochmanski, J. Nowacki, Surf. Coat. Technol. 202 (2008) 4834.

[6] S.D. de Souza, M. Kapp, M. Olzon-Dionysio, M. Campos, Surf. Coat. Technol. 204 (2010) 2976.

[7] J. Bielawski. J. Baranowska, K. Szczecinski, Surf. Coat. Technol. 200 (2006) 6572.

[8] Yucel Birol, Eng. Failure Anal. 26 (2012) 203.

[9] F. Ashrafizadeh. Surf. Coat. Technol. 173~174 (2003) 1196.

[10] C.X. Li, T. Bell, Corrosion Science 48 (2006) 2036.

[11] Y. Li, L. Wang, D. Zhang, L. Shen, Applied Surface Science, 256 (2010) 4149.

[12] R.F. Liu, M.F. Yan, Mater. Des. 31 (2010) 2355.

[13] W.P. Tong, N.R. Tao, Z.B. Wang, J. Lu, K. Lu, Science 299 (2003) 686.

[14] G. J. Li, J. Wang, Q. Peng, C. Li, Y. Wang, B. L. Shen, J. Mater. Proc. Technol. 207 (2008) 187.

[15] C.X. Li, T. Bell, Corrosion Science 46 (2004) 1527.

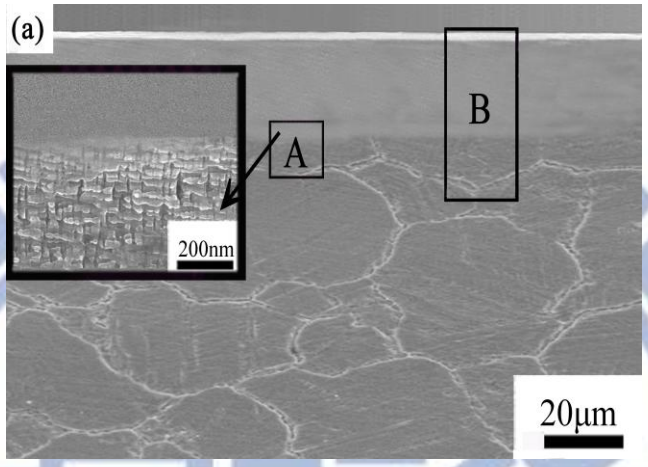

Figure 3.1(a)

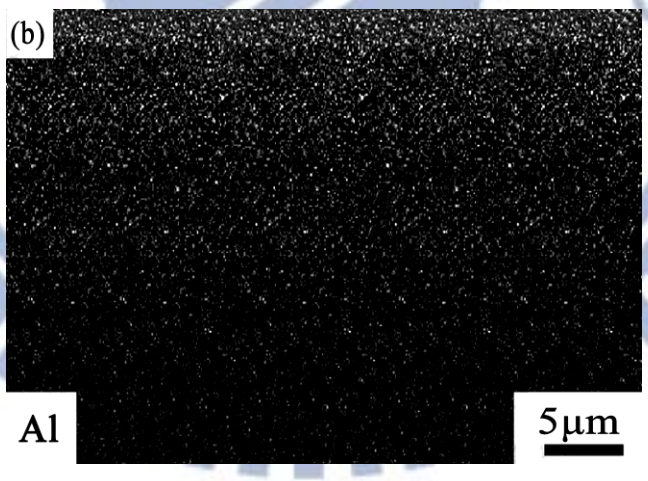

Figure 3.1(b)-(Al mapping)

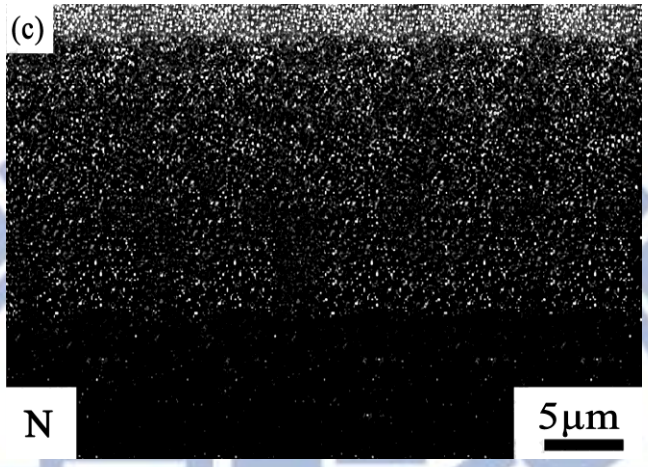

Figure 3.1(c)-(N mapping)

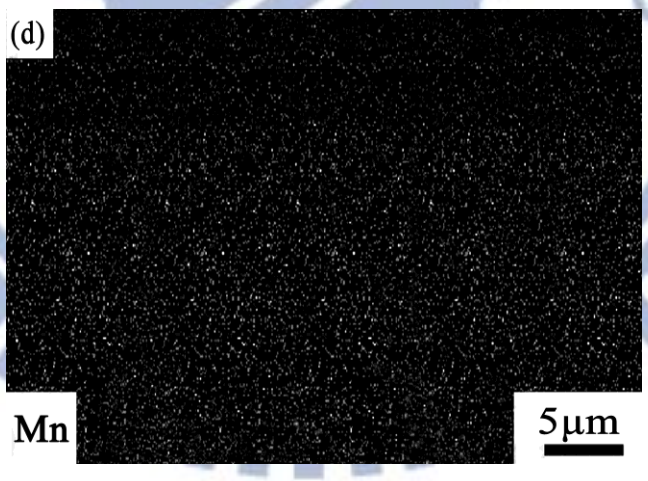

Figure 3.1(d)-(Mn mapping)

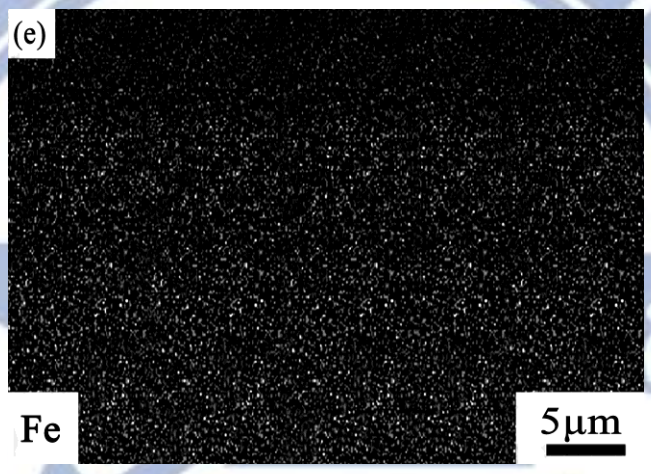

Figure 3.1(e)-(Fe mapping)

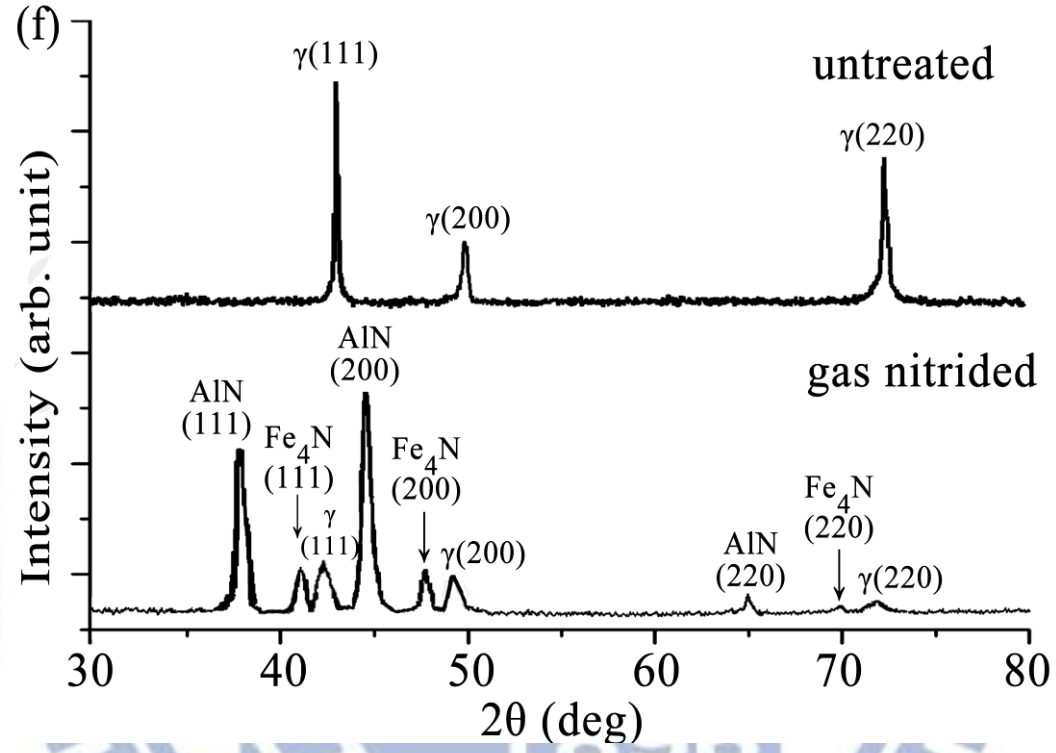

Figure 3.1(f)

Figure 3.1 (a) SEM cross-sectional image of the gas-nitrided alloy. Inset image shows the enlarged microstructure near the interface. (b) ~ (e) The elemental mapping images taken from the rectangular region marked in (a) for Al、 N、Mn and Fe, respectively. (f) XRD results for as-quenched and nitrided alloys.

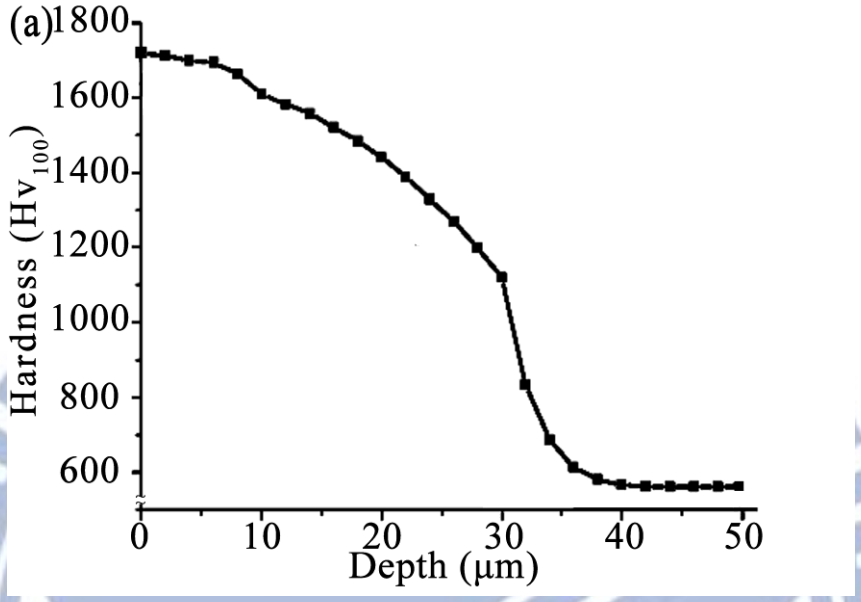

Figure 3.2(a)

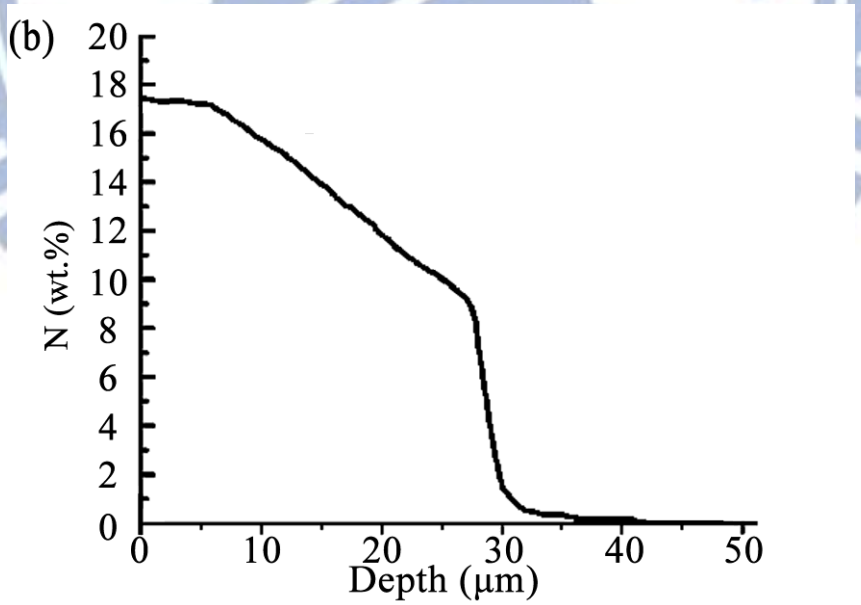

Figure 3.2(b)

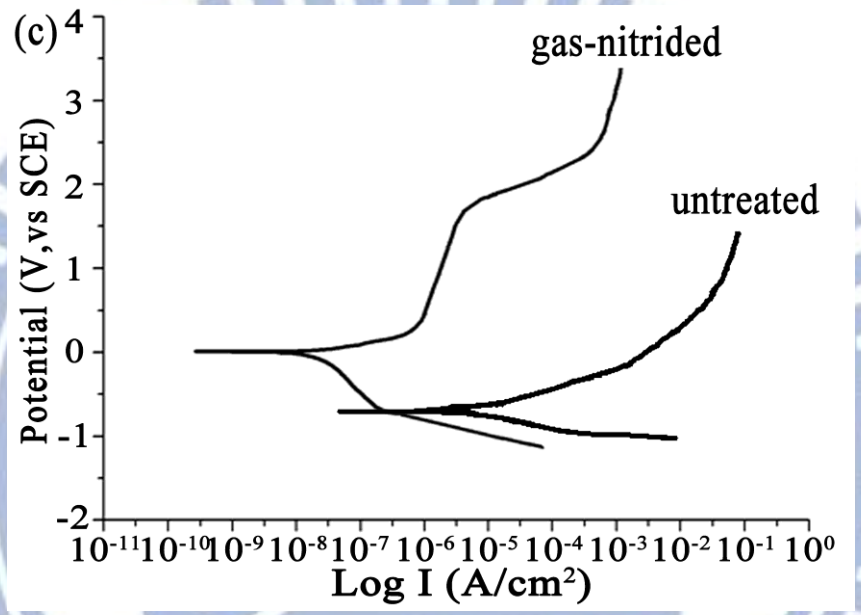
(c)
gas-nitrided
untreated
Potential (V, vs SCE)
4
3
2
1
0
-1
-2
10-11 10-10 10-9 10-8 10-7 10-6 10-5 10-4 10-3 10-2 10-1 100
Log I (A/cm2)

Figure 3.2(c)

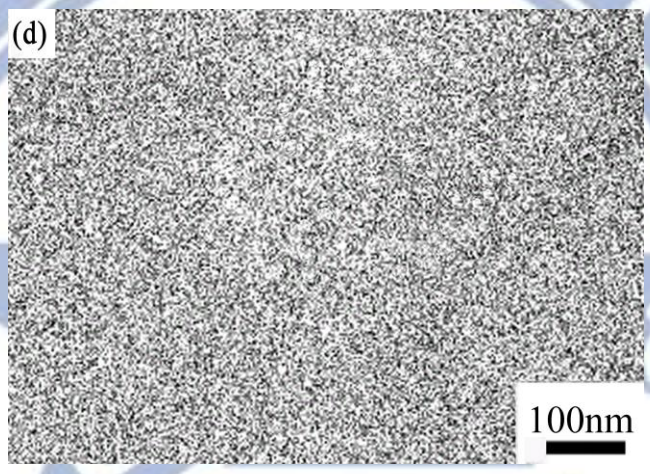

Figure 3.2(d)

Figure 3.2 (a)Nitrogen concentration profile of the present gas-nitrided alloy. (b)Hardness profile of the present gas-nitrided alloy. (c) Polarization curves for the present as-quenched and gas-nitrided alloys in 3.5% NaCl solution. (d) SEM surface image of the gas-nitrided alloy.

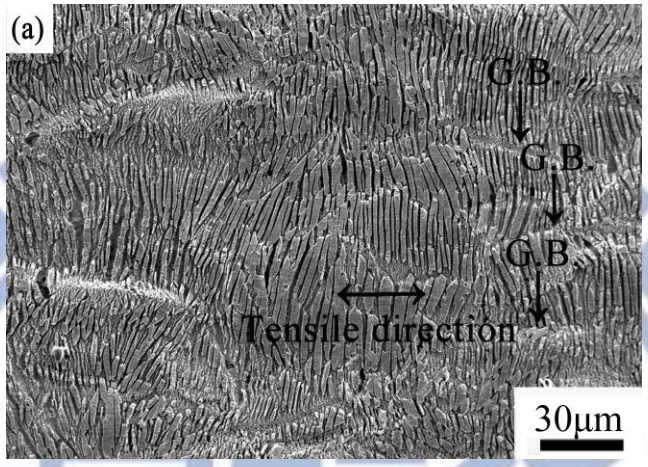

Figure 3.3(a)

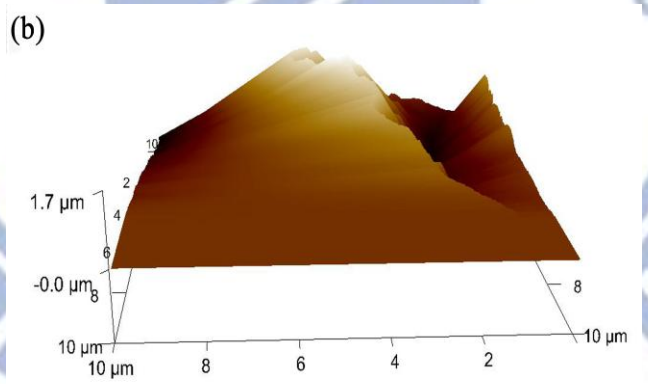

Figure 3.3(b)

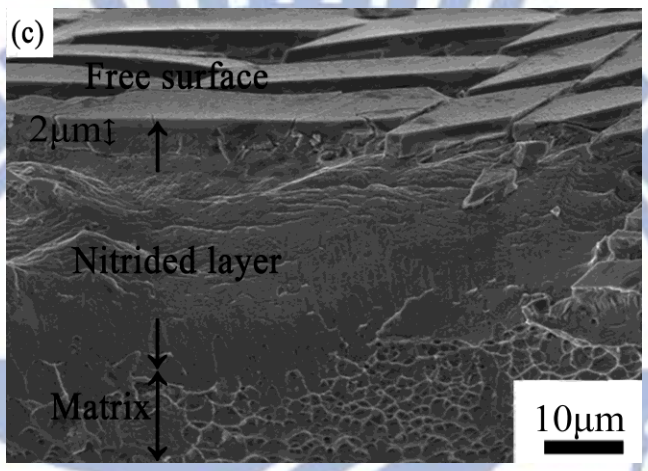

Figure 3.3(c)

Figure 3.3 (a) SEM image of the free surface of gas-nitrided alloy after tensile test. (b) AFM image of one of the fractured fragment. (c) SEM image of the fractured surface taken by slightly tilting the sample.

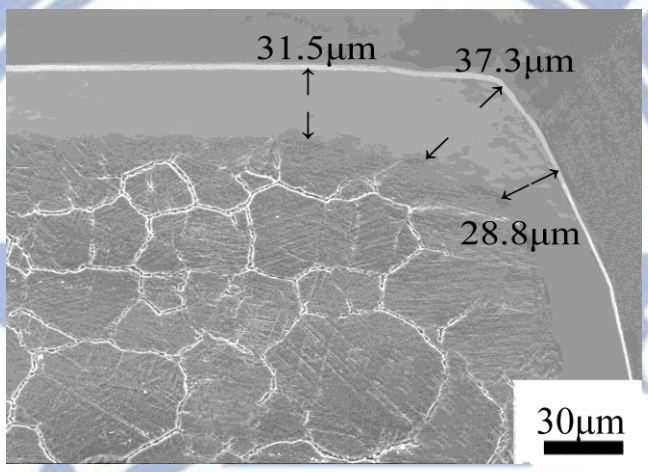

Figure 3.4

Figure 3.4　SEM image of the nitrided layer near the corner.

Chapter 4.

Summary

In the present study, both of the Fe-8.68wt.%Al-30.5wt.%Mn-1.85wt.%C and Fe-9wt.%Al-28wt.%Mn-1.8wt.%C alloy were plasma-nitrided and gas-nitrided at 500°C for 8h, respectively. After nitriding, the microstructures, mechanical properties and corrosion behaviors in 3.5% NaCl solution of the plasma-nitrided and gas-nitrided alloys have been examined. Based on the experimental results, some conclusions are given as follows:

[1]. The as-quenched microstructure of the Fe-8.68wt.%Al-30.5wt.%Mn-1.85 wt.%C alloy is ductile γ phase containing an extremely high density of nano-sized κ′-carbides formed through spinodal decomposition during quenching. The as-quenched alloy is plasma nitrided at 500°C for 8h resulting in the effects of aging and nitriding simultaneously. Furthermore, the resultant 40 μm-thick nitrided layer is composed predominantly of AlN with a small amount of Fe_4N. The nitrogen concentration at surface is extremely high up to 17 wt.% (41at.%). Consequently, the surface microhardness (1860 Hv), substrate hardness (550 Hv), ductility (33.6%) and corrosion resistance in 3.5% NaCl solution of the Fe-8.68wt.%Al-30.5wt.% Mn-1.85wt.%C nitrided alloy are far superior to those obtained previously for the optimally nitrided high-strength alloy steels as well as martensitic and precipitation-hardening stainless steels.

[2]. An extremely high density of nano-size κ′-carbides could be observed within the γ matrix. When the as-quenched alloy was directly gas-nitrided at 500°C for 8h, the size and amount of the κ′-carbides increased dramatically. Therefore, the nitrided alloy can possess exceptional combination of strength and ductility. Additionally, a ~30 μm-thick nitrided layer was found on the surface. Due to contain high content of strong nitride-forming element Al, the nitrided layer consists predominantly of nano-crystalline AlN with a small amount of Fe_4N in the as-quenched Fe-9wt.%Al-28wt.%Mn-1.8wt.%C alloy after being gas-nitrided at 500°C for 8h, The resultant nitrided layer accounts for the large surface microhardness (~1700 Hv), and the superior corrosion resistance in 3.5% NaCl solution, as well as the coherent and adhesive fracture behavior obtained. Moreover, gas nitriding appears to yield more uniform nitrided layer without suffering the edge effects.

[3]. After being nitrided at 500°C for 8h, the surface hardness, substrate hardness, ductility and corrosion behaviors in 3.5% NaCl solution of the plasma-nitrided Fe-8.68wt.%Al-30.5wt.%Mn-1.85wt.%C and gas-nitrided Fe-9wt.%Al-28wt.%Mn-1.8wt.%C alloy are far superior to those of optimally plasma-nitrided or gas-nitrided alloy steels, as well as martensite stainless steels and precipitation hardening steels.

List of Publications

Journal Papers

1. P.C. Chen, C.G. Chao and T.F. Liu, ”A novel high-strength , high-ductility and high-corrosion-resistance FeMnAlC low density alloy”, Scripta Mater. 68 (2013) 380-383.
2. P.C. Chen, C.G. Chao and T.F. Liu, “Structure and properties of gas-nitrided nanostructured Fe-9Al-28Mn-1.8C Alloys”, accepted for publication in Materials Chemistry and Physics (Aug. 2013).

Conference Papers

1. Y.X. Duan(段逸軒)、P.C. Chen(陳柏至)、X.L. Lin(林欣龍)、 Z.L. Lin(林志龍)、C.S. Wang(王承舜)、C.G. Chao(朝春光) and T.F. Liu(劉增豐), "Grain boundary precipitation in Fe-30Mn-9Al-5Cr-0.7C alloy", Proceedings of The 2008 Annual Conference of The Chinese Society for Materials Science.
2. 張凱明、陳柏至、林志龍、段逸軒、蔡國棟、劉亮延、王浩仰、朝春光、劉增豐, "鐵-9 鋁-30 錳-2 碳合金之顯微結構與機械性質", Proceedings of The 2009 Annual Conference of The Chinese Society for Materials Science.
3. 王喬立、陳柏至、王浩仰、張凱明、林志龍、段逸軒、朝春光、劉增豐, "鐵-9 鋁-30 錳-6 鉻-1.8 碳合金之顯微結構與抗腐蝕性質", Proceedings of

The 2010 Annual Conference of The Chinese Society for Materials Science.

4. 王承舜、林志龍、張凱明、陳柏至、林晟毅、孔睦穎、陳思漢、朝春光、劉增豐, "鐵-8.5 鋁-30 錳-1.0 碳合金之機械性質",台灣鑄造學會 2011